NRL Memorandum Report 6367

Turbulence Near a Free Surface in a Plane Jet

S. E. RAMBERG

Ocean Technology Program
Office of Naval Research

T. F. SWEAN, JR.

Center for Hydrodynamic Developments
Laboratory for Computational Physics and Fluid Dynamics

M. W. PLESNIA

Mechanical Engineering Department
Stanford University

March 14, 1989

SECURITY CLASSIFICATION OF THIS PAGE

ADA206269

REPORT DOCUMENTATION PAGE

Form Approved
OMB No 0704-0188

1a REPORT SECURITY CLASSIFICATION UNCLASSIFIED	1b RESTRICTIVE MARKINGS
2a SECURITY CLASSIFICATION AUTHORITY	3 DISTRIBUTION/AVAILABILITY OF REPORT Approved for public release; distribution unlimited.
2b DECLASSIFICATION/DOWNGRADING SCHEDULE	
4 PERFORMING ORGANIZATION REPORT NUMBER(S) NRL Memorandum Report 6367	5 MONITORING ORGANIZATION REPORT NUMBER(S)
6a NAME OF PERFORMING ORGANIZATION Naval Research Laboratory 6b OFFICE SYMBOL (If applicable) Code 4430	7a NAME OF MONITORING ORGANIZATION
6c ADDRESS (City, State, and ZIP Code) Washington, DC 20375-5000	7b ADDRESS (City, State, and ZIP Code)
8a NAME OF FUNDING/SPONSORING ORGANIZATION Office of Naval Research 8b OFFICE SYMBOL (If applicable)	9 PROCUREMENT INSTRUMENT IDENTIFICATION NUMBER
8c ADDRESS (City, State, and ZIP Code) Arlington, VA 22217	10 SOURCE OF FUNDING NUMBERS PROGRAM ELEMENT NO 61153N; PROJECT NO; TASK NO RR023-01-41; WORK UNIT ACCESSION NO DN158-016

11 TITLE (Include Security Classification)
Turbulence Near a Free Surface in a Plane Jet

12 PERSONAL AUTHOR(S)
Ramberg,* S.E., Swean, T.F., Jr. and Plesnia,** M.W.

13a TYPE OF REPORT	13b TIME COVERED	14 DATE OF REPORT (Year, Month, Day)	15 PAGE COUNT
Interim	FROM 10/87 TO present	1989 March 14	52

16 SUPPLEMENTARY NOTATION
*Ocean Technology Program, Office of Naval Research
**Mechanical Engineering Department, Stanford Univeristy

17 COSATI CODES			18 SUBJECT TERMS (Continue on reverse if necessary and identify by block number)
FIELD	GROUP	SUB-GROUP	Surface jet; Confined jet; Turbulent jet; Two-dimensional; Free surface

19 ABSTRACT (Continue on reverse if necessary and identify by block number)

Laboratory measurements of the turbulent flow in a plane jet issuing at the free surface are reported and analyzed. Single point hot-film data were obtained for mean velocities and turbulent fluctuations of velocity and shear stress in the developing jet to $x_1/b_0 = 240$ with an emphasis on the near surface turbulent behavior. Synoptic behavior of the jet resembled that of a 2D wall jet rather than one half of a planar free jet with the free surface represented by the symmetry plane. The effects of jet confinement are to retard the ability of the jet to entrain fluid, to decrease the growth rate of the length scale and to increase the decay rate of the velocity scale. Mean velocity

(Continues)

20 DISTRIBUTION/AVAILABILITY OF ABSTRACT ☒ UNCLASSIFIED/UNLIMITED ☐ SAME AS RPT ☐ DTIC USERS	21 ABSTRACT SECURITY CLASSIFICATION UNCLASSIFIED
22a NAME OF RESPONSIBLE INDIVIDUAL T.F. Swean, Jr.	22b TELEPHONE (Include Area Code) (202) 767-2114 22c OFFICE SYMBOL Code 4430

DD Form 1473, JUN 86 Previous editions are obsolete SECURITY CLASSIFICATION OF THIS PAGE

S/N 0102-LF-014-6603

SECURITY CLASSIFICATION OF THIS PAGE

19. ABSTRACT (Continued)

profile similarity is still observed when the data is non-dimensionalized with the reduced scales. Jet momentum will appear to have been lost due to momentum exchange with the return flow. An approximate analysis provides a means to estimate the momentum loss due to limited depth and is shown to correlate well with scale development in several jet configurations for these and prior experiments. One-dimensional turbulence spectra revealed "blocking" of certain vertical scales as the free surface is approached with a concommitant redistribution of turbulent kinetic energy from the vertical fluctuations to the lateral components. This is in qualitative agreement with recent analyses and experiments for isotropic turbulence near moving walls and free surfaces but differs by exhibiting a wider range of surface-influenced turbulent length scales and a thinner influenced layer below the free surface.

DD Form 1473, JUN 86 (Reverse)

CONTENTS

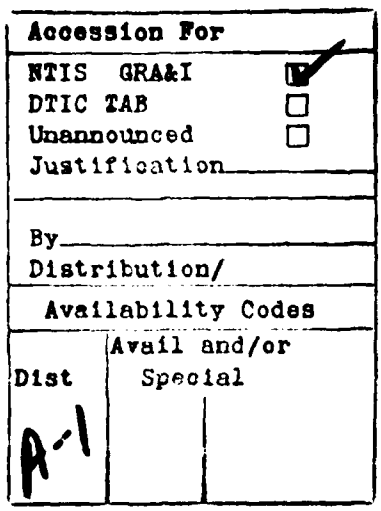

TURBULENCE NEAR A FREE SURFACE IN A PLANE JET

INTRODUCTION

The turbulent flow below a gas-liquid interface plays an important role in diverse areas ranging from environmental flows and industrial mixing processes to the remote sensing of ship wakes. The near-boundary influences upon transfer and diffusion at the interface is of primary concern in environmental and industrial applications whereas remote sensing issues ultimately involve any surface motions which may be detectable. The remotely sensible surface events may be either generated or modified by the subsurface turbulent flow. The primary motivation for the present work stems from the remote sensing problem wherein various sensors appear to respond to the turbulent wake region of a surface ship wake. For example, the two most common and persistent features seen in synthetic aperture radar (SAR) images of ship wakes include bright "narrow-vees" and long dark "scars" which may be a result of surface Bragg wave generation or modification through interactions with near surface turbulence. Common to all of these problems is the need for a better understanding of the structure of turbulence below a free surface. The present study experimentally examines the turbulent structure below a free surface where the underlying flow is developing in the manner of a 2D planar jet. Surface deflections are minimized in order to isolate the kinematic effect of the free surface upon the turbulence below. Future studies will begin to examine the interaction of the underlying turbulence with the surface motions.

BACKGROUND

The literature on bounded shear flows is extensive but almost exclusively directed at the boundary layer problem where the no slip boundary condition leads to steep velocity gradients very near to the boundary and a nonzero shear stress at the wall. A clean free surface with neglible velocities in the overlying gas phase cannot support a mean or fluctuating shear stress and therefore, unlike the classical boundary layer flow, turbulence is not produced at or near to the boundary. The surface region acts to modify and to dissipate the impinging turbulence which has been generated below and advected to the surface. This simple characterization of a free surface is usually complicated in practice by the presence of surfactant or other contaminating material on the interface which moves freely in the mean but supports a fluctuating shear stress. Further practical complications include the possibilities of significant gas flow and of interfacial deflections. As noted above the remote sensing problem is a consequence of

Manuscript approved September 22, 1988.

the surface motions and in that instance the interactions of the surface waves with the turbulence must ultimately be considered. Extreme surface agitation with spray production and/or gas bubble entrainment is also important in a variety of environmental and industrial processes but is beyond the present treatment.

Since the density and viscosity of the overlying gas phase are expected to be much smaller than for the liquid, considerably larger gas than liquid velocities are required to produce a significant applied shear. However, relatively small gas velocities in an overlying turbulent flow can give rise to small amplitude surface waves by virtue of turbulent pressure fluctations convected in phase with the wavelets (Phillips, 1969). This mechanism can also be expected to generate waves from the turbulent pressure fluctuations below if matches exist between the wave phase speeds and the fluid convection velocity of appropriate turbulent "eddy" scales. However, a lower limit exists for wave generation of this type since a minimum phase speed for gravity-capillary waves can be determined to be about 20 cm/sec depending on the value of surface tension. For most of the present configuration the mean velocities are below this limit. Unsteady generation of waves by uncoupled pressure fluctuations is also possible but are expected to produce much lower amplitudes.

Surface contamination is expected in all but very carefully controlled laboratory conditions. The presence of such materials means that fluctuating shear stresses can be nonzero at the interface. In the limit of a very contaminated surface, which may be more the rule than the exception, the turbulent velocity fluctuations in the plane of the surface are completely suppressed (c.f. - Levich, 1962). Under the assumption of neglible vertical surface motions, the free surface behaves like a rigid wall moving at the free stream velocity such that mean shear is zero but the fluctuating shear is not. These conditions were employed by Hunt (1984) to apply a theory for a moving wall (Hunt & Graham, 1978) to the free surface problem. In this theory, isotropic decay of turbulence behind a grid is taken as the outer or farfield source of turbulence for interaction with a wall moving at the speed of the free stream. The theory describes a layer near the surface where vertical turbulent scales larger than the distance to the surface are blocked which produces an anisotropic redistribution of turbulent energy from the vertical (x_2) component to the two lateral components. The thickness of the redistribution layer is on the order of the farfield turbulent integral scale, L_0. The turbulence kinetic energy is shown to be equal to its farfield value as $x_2/L_0 \rightarrow 0$ and for $x_2/L_0 \rightarrow \infty$. The equality does not hold for all x_2/L_0 since the kinetic energy exhibits a minimum within the region associated with a rise in mean pressure.

Measurements of the grid turbulence in proximity to a moving wall by Thomas & Hancock (1977) and computations of a similar flow by Biringen & Reynolds (1981) are in general agreement with the theory. Related experiments for an oscillating grid below a rigid wall by McDougall (1979) and below a free surface by Brumley & Jirka (1987) also generally agree with the theory. The blocking of vertical scales as the surface is approached and the redistribution of turbulent energy from vertical to lateral components are observed in all of the above cases although not exactly as the theory predicts. Differences from the theory include greater anisotropy among turbulent

components and a wider range of surface influenced turbulent scales. These differences have been ascribed to the modification of the finer scales of the turbulence by the larger surface-influenced scales which is expected but not included in the theory.

All of the above literature is restricted to a farfield or source turbulent flow which is isotropic and therefore characterized by a single farfield integral scale. The present study was undertaken to examine a nonisotropic turbulent farfield in the presence of a free surface. The basic flow chosen for this investigation was a nominally two-dimensional planar jet issuing at a free surface, often termed a surface jet.

Considerable literature has been generated in the study of jet behavior for a variety of bounded and free geometries. Relatively little attention has been given to surface jets except for the hydraulic literature where the concern is for the influence of buoyancy on the spreading and mixing of outfalls that are generally warmer than the receiving fluid. A study by Chu & Baddour (1984) presents experimental results for a buoyant planar jet and contains a good review of that particular area of the literature. They show that very small density differences (low Richardson numbers) have a pronounced influence on jet entrainment, and hence jet behavior, which renders most of that literature of little value to the present problem. Indeed, the few experimental results presented for neutrally buoyant jets as part of those studies may be suspect due to facility constraints on the entrainment. This is discussed later in this report.

Rajaratnam (1976) has collected most of the available data and analyses on non-buoyant conventional jets, including both planar and axisymmetric geometries, and with and without an adjacent wall boundary. Some experimental results for more general three-dimensional jets and other effects are also included. No surface jet results or analysis are described therein but Rajaratnam (1984) has reported experimental data for both planar and axisymmetric surface jets where it is shown that mean velocity profiles exhibit similarity based on the usual characteristic velocity and length scales. For the planar surface jet these scales vary in a manner closest to the planar wall jet where the jet issues tangent to the wall. This geometry is similar to the surface jet whereby the free surface is replaced by a rigid wall and both of these configurations are geometrically similar to the unbounded planar jet where the plane of symmetry is replaced by either the wall or the free surface. The various geometries are sketched in Fig. 1. Earlier results by Rajaratnam (1969) indicated that the surface jet synoptic scales behaved more like the free planar jet scales but it is likely that those results were influenced by jet confinement wherein the the limited depth of the facility inhibited entrainment and therefore affected the observed jet behavior in a manner analagous to the buoyant jets.

The influence of confinement upon jet entrainment and behavior has been the source of some controversy in the interpretation of often conflicting reports of measured jet behavior. The conflicts become most apparent in consideration of the integrated momentum flux variation along the jet and its relation to the rate of entrainment. The data for free jets obtained by Goldschmidt and Eskinazi (1966), Heskestad (1965), Miller and Comings (1957), and Kotsovinos (1975), as collected by Kotsovinos (1978) all show significant momentum losses within 160 slot-widths downstream. Kotsovinos

(1978) estimated the various terms in the momentum equation and concluded that jet momentum is lost in the interaction with the induced outer flow. Schneider (1985), with a more formal argument, has provided a reconciliation of many discrepancies by coupling an analysis of the jet development to the outer flow. The analysis is developed for a submerged turbulent planar jet but the major features should be equally applicable to the surface jet under the analogy between a free surface and the plane of symmetry for the submerged jet. This analogy is not always valid but appears appropriate to this discussion. The analysis predicts that the jet half width scale variation will not be affected by the confinement but the velocity scale will no longer vary as $x_1^{-1/2}$ (x_1 =primary flow direction) which is the classical similarity result. In fact, the maximum velocity will decrease more rapidly and momentum will appear to have been lost.

EXPERIMENTAL METHODS AND PROCEDURES

The experiments reported here were performed at one end of a long tow channel (Fig. 2) described by Ramberg and Fung (1982). The channel has nominal interior dimensions of 1 m in depth, 1.3 m in width and 18 m in length. In the early stages of this work a false bottom was in place on the floor of the channel and the dimension h was 51 cm. This was later removed and in the final experiments $h = 82$ cm. The temporary dividing wall was located 46 cm from the near wall and in the final configuration extended downstream to 2.62 m. The water level in the channel was maintained by a steady supply of water at one end and an adjustable overflow drain at the opposite end. The jet flow was obtained by replenishing the jet reservoir with water from the far end of the channel. Both flow rates were monitored along with the mean and still water depths over the jet lip ($x_1/b_0 = 0$). As a result of these precautions, the discharge height of the jet ,b_0, and the still water level were maintained to within 0.02 cm or about 2% of the initial jet height. Figure 2 also contains the nomenclature for describing the results. Subscripts are used to denote the three coordinate directions where the primary flow is in the "1" direction and the vertical down direction is "2", leaving "3" for the transverse or lateral direction in a right-handed coordinate system. Conditions at the jet inlet ($x_1 = 0$) are denoted by the subscript $(\ )_0$ and locally maximum values are designated by the subscript $(\ )_m$. The time-average of the i^{th}-component of velocity is denoted by U_i and its velocity of fluctuation by u_i'. In the discussion that follows the primes will be omitted from the fluctuating velocities and mean values of turbulence quantities will be denoted simply by an overbar. We further use the short-hand notation $\overline{u_i}$ to denote $(\overline{u_i'^2})^{1/2}$.

The data were obtained with a dual sensor hot film probe (DISA 55R62) connected to DISA 56C01 constant temperature anemometers. The anemometer output voltages were passed through DISA 56N21 linearizers then through DISA 56N20 signal conditioners where they were offset to $\pm$5v for acquisition by a QSI simultaneous sample digital tape recorder. Prior to recording, the signals were filtered through Rockland Wavetek Model 452 filters. The sensors were mounted on a vertical and horizontal traversing system operated by a Velmex Model 8300 controller, which was in

turn mounted on one of the tow channel carriages. The elements were operated at an overheat ratio of 1.06 to prevent bubble formation.

Probe fouling by contaminants is a significant problem when making hot-film measurements in water. This has been observed by numerous researchers and elaborate techniques have been developed in attempts to overcome the problem (e.g., Hubbard, 1985). In the experiments described here, water impurities were kept to a minimum by constant filtration and recirculation during periods when a measurement was not in progress. In addition a drain was positioned at the far end of the channel, approximately 12 m from the downstream end of the test section. The height of the drain was adjustable and was typically positioned to very slowly but constantly remove the free surface. Water velocities induced by this technique were too small to be measurable. Nonetheless, there would remain some voltage drift due to contamination which necessitated frequent calibrations of the sensors. Before and after each measurement run the tow carriage was stepped through ten speeds covering the jet velocity range. This calibration data was digitized and stored in a file on the data tape as well as read directly into a local computer (HP 1000/A600) in the laboratory. In this way calibration constants could be established for the linear probe outputs and these could be checked for consistency during a long series of measurement stations. Typically the calibrations would drift slowly due to accumulation of material on the sensors. When necessary, gentle brushing of the elements would restore the sensitivities to original values, after which the sensors would "season" over a short time and exhibit a voltage drop of a few percent. This would be followed by the very slow drift behavior. When this nearly steady-state condition was established the probes were operated in the slow drift mode while monitoring the calibrations from run to run. For long periods a near-equilibrium condition would be established and as much data under this condition as possible was recorded. The run-times for a set of measurements were typically 30-60 min over which time the output voltages could be expected to drift on the order of 3-5% (slope change of linearized output). The data were ultimately reduced by assuming a time-linear drift and weighting the data to the before-and-after calibrations according to the time they were obtained. Typical linearized voltage/velocity calibration curves are shown in Fig. 3.

Discrete probe contamination events were encountered each time the elements passed through the free surface and sometimes when located in the low speed, intermittent flows near the edge of the jet (on the bottom). To avoid these events vertical profiles of flow quantities were obtained by two separate sequences of probe positions under control of the traversing system. Both sequences started and ended at the elevation of the jet lip with one being down and back and the other up through the free surface and back. These were performed separately and the two sets of data were combined to give the results presented in this and the next sections. Two probe orientations were used to obtain all three velocity components with the x_1 components common to both orientations. The measurement sequence that approached and then passed through the free surface would produce a local disturbance in the free surface about the probe prongs. The result was flow about the sensor elements above the mean

water level in the absence of the probe. Data recorded in this region were ignored but indicates the limitations of an intrusive measurement.

Composite profiles were obtained at ten axial stations along the centerline of the developing jet ($x_3 = 0$ in Fig. 2). The flow field was checked at several of these stations to insure two-dimensionality in the mean velocity field. Figure 4 is typical of these measurements and shows that the wall effects are negligible over at least the innermost 50% of the test section. At each station the sequence of vertical positions and dwell time for each were programmed into the traverse control. The microprocessor within the controller also operated the digitizer and tape drive to generate files corresponding to each position in each station profile. The sampling rates per channel and the typical record lengths varied with longitudinal position in the jet as listed in Table 1.

Table 1. Sampling Rate and Record Length

x_1/b_0	Rate (Hz)	Time (sec)
0	200	45
4	200	45
20	200	65
40	200	65
60	200	65
80	200	65
120	100	65
160	100	120
200	100	120
240	100	120

For the final jet configuration, each profile was repeated at least twice for each sequence of each probe orientation so primary directions were realized at least six times and the others four times. The results are the averages of the individual realizations at each point.

A number of additional problems were encountered during the experiments stemming from the finite dimensions of the facility and the free surface. In an effort to obtain the largest possible initial jet velocity U_0 it was necessary to operate the facility just below an exit Froude number of unity. This produced a steady wave pattern in the early portion of the jet as shown in Fig. 5. The data shown in the figure were obtained by manual probe positioning to locate the mean free surface position visually for both the operating jet and the still basin in order to discount variations in the carriage track elevation. In addition to the steady waves it is clear that a mean surface slope existed over much of the jet region of interest. Similar behavior was indicated in the first set of results for a planar surface jet reported by Rajaratnam (1969). The pressure gradient implied by this variation seems a natural consequence of the return flow required along the bottom of the channel to supply the entrained fluid from elsewhere in the basin and is a reflection of the opposing momentum established in the entrained fluid. The

presence of steady surface waves early on can also be expected to alter the initial development region through the imposition of oscillatory perturbations of the spreading shear layer emanating from the lip of the jet. We have assumed this influence is local and unrelated to the farfield behavior except perhaps as a shift in the jet virtual origin.

The stability and the accuracy in the results due to these procedures are indicated by the data shown in Figs. 6a and 6b. These data were taken as longitudinal sequences along the jet at a fixed depth below the free surface ($x_2 = 0.15\ cm$). The different symbols correspond to the two probe orientations and two separate dates of the sequences. The first date was at the outset of the experimental program with the final jet configuration and the second at its conclusion. The horizontal scale is expanded in the early portion of the jet. The growth of the shear layer into the fully formed jet and the presence of the steady surface waves are apparent. Isotropy in the very low turbulence above the spreading shear layer is seen for $x_1/b_0 < 6$ which rapidly becomes larger and anisotropic as the shear layer spreads past the probe elevation and eventually reaches the free surface. Thereafter the mean and turbulent quantities decay as the jet spreads. The effect of the free surface on the turbulent fluctuations can be seen from this data in the farfield. The vertical component $\overline{u_2}/U_0$ is decaying more rapidly than either of the lateral components which are becoming more comparable in magnitude. Early in the jet the longitudinal component dominated and the other two were more comparable. This is the redistribution of turbulent kinetic energy into the lateral fluctuations at the expense of the vertical motions which is the anisotropy mechanism introduced by the presence of the free surface. Prior to a full discussion of the free surface phenomena, the major objective for this study, it is necessary to first discuss some aspects of preliminary experiments which led to the final jet configuration.

PRELIMINARY EXPERIMENTS

A number of preliminary experiments were performed with various geometries and jet flow rates in search of an arrangement where proper jet behavior could be maintained at large x_1/b_0. The goal was a farfield linear variation in the characteristic jet length scale, $b(x_1)$, and a farfield variation in the characteristic velocity scale $U_{1_m} \sim x_1^{-1/2}$. There were difficulties in achieving these behaviors which stemmed from the large entrainment associated with jets and the restrictions placed on the necessary bottom return flow by the finite depth. The confinement effect was not obvious in the initial hot film data and was only revealed by flow visualization and by examination of the above scale variations and by examination of the momentum balance in the developing jet. For the large downstream distances which we sought to employ, the jet entrains nearly four times the volume flow rate issued at the jet discharge. If the depth of the jet becomes an appreciable fraction of the total depth within the channel then the return flow velocity field is comparable in both extent and magnitude to the jet itself. As this condition is approached in the developing jet, the source direction of entrained fluid has a growing component opposite to the jet flow which carries oppositely signed momentum into the jet. In extremis, the jet attaches to the floor of the channel, a recirculation cell is formed below the jet and the overall pattern resembles the flow over

a rearward facing step. Between the proper jet mode and this recirculating cell mode various combinations of geometry and flow rates yield three dimensional and sometimes unsteady combinations of the two modes. These deviations of real jets from unconfined jet behavior are often subtle and can easily be overlooked. All jets exhibit an initial development region and if this is immediately followed by spreading under the influence of limited entrainment then it is likely that the proper scale variations will never be seen in the data. Profile similarity is still observed for these confined jets and one is easily misled unless conservation of momentum is also examined. The pathological behavior is also masked by the usual weaknesses inherent with hot-film measurements in regions of low velocity (jet edges) and the sensor directional insensitivity in regions of reversed flow.

Kotsovinos (1978) with an approximate procedure and, more formally, Schneider (1985) have shown unequivocally that a 2D jet issuing from a wall must suffer a loss of momentum. This is at variance with the classical boundary layer solution which does not account for the presence of the upstream wall and fails to predict a component of entrainment momentum which is in the direction opposite to the main jet flow. For a plane turbulent jet issuing from a vertical upstream wall, Schneider's analysis predicts that the momentum, J, will slowly vary as

$$\frac{J}{J_0} = \left(\frac{x_0}{x_1}\right)^{\epsilon_e/2} \tag{1}$$

where $\epsilon_e = 0.085$ for a 2D turbulent jet, and x_0 is a constant of integration of $O(b_0)$ such that $J/J_0 = 1$ at $x_1 = x_0$. Schneider's results differ from those of Kotsovinos by the values of the constants and the behaviors of the two theories as $x_1 \to \infty$. It is important to note that the theories account only for the upstream wall but it is reasonable to assume that the presence of a horizontal surface would further degrade the momentum since all entrained mass must originate from downstream. A measure of the effect of a confining horizontal surface can be obtained by examining the deviation of the developing jet from the behavior described by Eq. (1).

Rajaratnam and Humphries (1984) and Vanvari and Chu (1974) provide the only known studies of 2D non-bouyant surface jets prior to this research. Rajaratnam presents no results explicitly for the longitudinal momentum flux, although the flux could be deduced from reported velocity and length scale data, and Vanvari reports a 50% reduction in momentum flux by $x_1/b_0 \approx 62$. This is considerably more than that allowed by Eq. (1) and is undoubtably due to the finite channel depth. Vanvari postulates as much and further notes a breakdown in the linear growth of the jet width as early as $x_1/b_0 \approx 25$.

Our initial jet configurations exhibited the finite-depth induced breakdown at moderate $x_1/b_0 < 100$ and several steps were taken to rectify the situation. These included perforating the original false bottom and temporarily removing the upstream vertical wall at $x_1 = 0$ in order to allow additional sources for entrainment fluid. An estimate of the momentum loss due to the finite geometry can be obtained from a momentum

and mass balance applied to Fig. 7. It is desired to estimate the usable test length, L_e, given the facility constraint, h, and the controllable parameters U_0 and b_0. The determination should be subject to the additional constraint that the momentum loss due to finite depth be maintained within acceptable limits. Assuming the density is everywhere constant and neglecting momentum exchange at solid boundaries or the free surface, the momentum balance for the geometry of Fig. 7 is approximately,

$$U_0^2 b_0 - U_e^2 b_e = U_0^2 b_0 (1 - f) + U_r^2 (h - b_e), \tag{2}$$

and the mass balance is,

$$U_0 b_0 + U_r (h - b_e) = U_e b_e. \tag{3}$$

The first term on the right-hand-side of Eq. (2) is the expected loss due to the upstream wall as given by Schneider (1985) with f determinable from Eq. (1), and the second term is included to account for the fact that all entrained fluid must originate from downstream. It is further presumed that the velocity and length scales of the well-behaved jet should exhibit behaviors approximating,

$$\left(\frac{U_0}{U_{1_m}}\right)^2 = C_1 \left(\frac{x_1}{b_0}\right) + C_2 \Rightarrow \left(\frac{U_0}{U_e}\right)^2 = C_1 \left(\frac{L_e}{b_0}\right) + C_2 \tag{4}$$

and

$$\frac{b}{b_0} = C_3 \left(\frac{x_1}{b_0}\right) + C_4 \tag{5}$$

The above postulates are clearly subject to criticism due not only to the simplistic velocity profiles and other effects previously mentioned but also by noting that turbulence is only represented by the particular functionals of x_1/b_0 incorporated into Eqs. (1,4-5). Those equations are themselves somewhat inconsistent for finite x_1/b_0 since Eqs. (4-5) imply momentum is invariant in x_1 while Eq. (1) shows otherwise. Nevertheless, useful estimates can be obtained from the above relationships and their utility can be shown a posteriori. In principal all of the parameters b_e, U_e, U_r and L_e are determinable from the Eqs. (1-5) if values of the constants are assumed and the experimental conditions are stated. There results a complicated transcendental equation $L_e/b_0 = F(x_1/b_0)$ which satisfies the system to the degree one is willing to pursue the calculation. The result represents the length over which the jet has lost all momentum to the return flow. That calculation, however, is not pertinent to the experimental requirement that $U_r^2(h - b_e) \ll U_0^2 b_0 (1 - f)$ to represent acceptably mild losses due to the finite depth. In fact, since the momentum loss due to the vertical wall is only a slowly-varying function of x_1, it suffices to require,

$$\Delta_J \equiv \frac{U_r^2 (h - b_e)}{U_0^2 b_0} \ll 1. \tag{6}$$

If we further assume substantial x_1/b_0 such that the effects of the kinematic and geometric virtual origins (C_2, C_4) can be ignored, then there results from Eqs. (3-6),

$$C_3^2 C_1^{-1} \frac{L_e}{b_0} - 2C_3 C_1^{-\frac{1}{2}} \frac{L_e}{b_0}^{\frac{1}{2}} + 1 \approx \Delta_J \left(\frac{h}{b_0} - C_3 \left(\frac{L_e}{b_0} \right) \right).$$

The large majority of jet studies show that $C_3 \sim C_1$ so this can be further approximated to

$$(1 + \Delta_J) \left(\frac{C_1 L_e}{b_0} \right) - 2 \left(\frac{C_1 L_e}{b_0} \right)^{\frac{1}{2}} + \left(1 - \frac{\Delta_J h}{b_0} \right) \approx 0,$$

or

$$\left(\frac{C_1 L_e}{b_0} \right)^{\frac{1}{2}} \approx \frac{1 + \sqrt{\Delta_J (h/b_0 - 1 + \Delta_J)}}{1 + \Delta_J}, \tag{7}$$

where the physical solution has been retained. Consistent with large x_1/b_0 it is required $h/b_0 \gg 1$ and by necessity $0 \leq \Delta_J \leq 1$, then

$$\left(\frac{C_1 L_e}{b_0} \right)^{\frac{1}{2}} \approx \frac{1 + \sqrt{\Delta_J (h/b_0)}}{1 + \Delta_J}. \tag{8}$$

Since in the range $0 \leq \Delta_J \leq 1$ and for realistic h/b_0 there are no zeros of $dL_e/d\Delta_J$, it is clear that L_e increases with both Δ_J and h/b_0 as expected. This simply states the finite-depth induced momentum loss will stay within acceptable bounds for a greater downstream distance if the channel is made deeper. Conversely, for a fixed channel depth, the available distance for 'good' jet development decreases as the requirements on the bottom effect are tightened. Since we have restricted attention to $C_1 L_e/b_0 \gg C_2$ the result does not depend on the initial momentum flux. For moderate Δ_J and very large h/b_0 the result is independent of b_0. In this instance and assuming $C_1 \sim 0.1$ as is typical of jets and accepting a momentum loss of 10% then $L_e \approx h$.

Table 2 is a tabulation of the several jet configurations surveyed and Figs. 8a-b show the development of the scales in the low to moderate x_1/b_0 range. The table and figures also include data from other pertinent experiments. It is clear that jet 1 is beginning to show deviations in the velocity scale before $x_1/b_0 = 100$ and likely that is the case with jets 2 and 3 also. Each jet, however, is progressively becoming better behaved. Jets 1 and 2 showed the same tendencies in their length scale variations although the breakdown is not so evident until $x_1/b_0 > 100$. Detailed profiles were not taken for jet 3 but only in the higher h/b_0 range were we able to achieve the expected behaviors for substantially large values of x_1/b_0.

Table 2 also includes a tabulation of Eq. (8) under the constraint of 10% momentum loss. Although there is some Reynolds number effect, the jets surveyed under the present study have typically $C_1 \approx 0.05$ so only jet 1 could be expected to show obvious signs of breakdown within $x_1/b_0 \leq 100$. The studies of Rajaratnam (1984) and Vanvari and Chu (1974), however, both indicate values of $C_1 \approx 0.1$. In that case we might expect only the third jet of Rajaratnam to survive to $x_1/b_0 \sim 100$ without

incipient breakdown. Indeed of the four studies, only Rajaratnam's #1.3 can be considered free of bottom influence until $x_1/b_0 \sim 80$. Rajaratnam's #1.1 shows clear signs of breakdown between $55 \leq x_1/b_0 \leq 75$ and his #1.2 survives only slightly longer. The results of Vanvari and Chu appear to degrade beyond $x_1/b_0 = 50$. These numbers all are closely correlated with the calculations in Table 2 for L_e.

Table 2. Experimental Parameters

Reference/ Exp. No.		b_0 (cm)	$C_1 L_e/b_0$ $(\Delta_J = .1)$	h/b_0	U_0 (cm/sec)	Re $U_0 b_0/\nu$	Symbol Fig. 8
present study	1	3.30	4.16	15.45	46	14990	1
	2	1.78	5.99	28.65	43	7558	2
	3	1.27	7.46	40.16	40	5017	3
	4	0.66	11.81	77.27	34	2215	4
	5	0.97	8.96	52.58	39	3735	5
	6	1.42	9.57	57.75	42	5890	6
	7	1.42	9.57	57.75	42	5890	
	8	1.42	9.57	57.75	27	3786	
	9	0.79	14.73	103.80	31	2418	9
	10	0.76	15.17	107.89	34	2552	0
Rajaratnam (1984)	1.1	1.31	7.30	38.85	11	1431	■
	1.2	0.98	8.89	51.94	11.5	1119	◆
	1.3	0.64	12.06	79.53	10.8	686	▲
Vanvari & Chu (1974)		0.81	6.17	30.00	28.3	2675	⊠
Patel (1961)		0.51				30000	- - -△- - -
Tailland (1967)	1	0.60				11000	- - - + - - -
	2	0.60				18000	—— * ——
	3	0.60				25000	— -×— -
Guitton (1970)		0.77				30800	—— ◇ ——
Ramaprian (1985)		0.25			30	741	—— □ ——

Also shown in the Figs. 8a-b are mean lines through data typical of two-dimensional free and wall jets. The surface jet development is expected to more closely follow that of a wall jet than a free jet which is the trend of the present data. Recent flow visualization of the entrainment patterns in an axisymmetric free jet by Shlien (1987) exhibited full jet width intrusions of outer entrained fluid from one side of the jet. Like a wall jet, these intrusions will be halved in a surface jet and on that basis these two configurations would be similar and distinguished from a free plane jet.

As seen in the figures our lower Reynolds number jets (4, 5, 9 and 10) exhibit perceptably faster growth in length scale and faster decay in velocity scale than our high Re jets (1, 2, 3 and 6). This is the same trend as shown in the wall jet data of Tailland (1967). The velocity decay is generally slightly slower for our jets than

the decay exhibited by the wall jets and the mean lines through the wall jet data of Guitton (1970) and Patel (1961) approximately interpolate the length scale growth rate of the present low Re jets. All of the wall jet data shown as well as the surface jet data of the present experiments lie significantly below the plane jet data which is typified by that of Ramaprian (1985). It should be pointed out that these wall jet studies are among those deemed acceptable for use in turbulence modelling by Launder and Rodi (1981). In that study Launder and Rodi surveyed more than 70 wall jet experiments and examined them for momentum conservation as well as other measures of internal consistency. In most of the experiments there was found to be a marked variation of momentum flux along the jet axis, usually a considerable momentum loss, of which only a relatively small portion could be attributed to friction losses at the wall. Those experiments showing substantially too great of a loss were excluded from further study and the studies referenced in Table 2 were among those retained. With the exception of the second experiment of Rajaratnam (1984) all of the velocity scale data of the non-bouyant surface jet studies (excluding the present data) are seen to lie above the plane jet and all are showing jet breakdown at moderate x_1/b_0. While it is less obvious in the length scale data, close scrutiny leads one to suspect those data are showing symptoms of breakdown as well. The length scale variation of the second experiment of Rajaratnam follows closely the plane jet behavior until suddenly breaking off around $x_1/b_0 = 50$. As mentioned in an earlier section with reference to Schneider's (1985) analysis, the effects of confinement should be manifest first in the velocity scale (momentum loss) and only later in the length scale variation. From this analysis and the results from our several experiments, we feel that it is likely that all of the Rajaratnam non-bouyant jet studies as well as the single experiment of Vanvari and Chu are contaminated by confinement effects. It is fair and proper to point out, however, that the latter effort had as its primary focus the study of bouyancy effects. The non-bouyant jets were limited observations to provide a basis to study the bouyancy effects. It is clear that effects due to bouyancy differences rapidly outweigh those due to confinement.

The final configuration chosen for the jet experiments, labeled as number 10 in Table 2, yielded the variations of $b(x_1)$ and $U_{1m}(x_1)$ shown in Figs. 9a-b. It should be noted that for $x_1/b_0 > 160$ the velocity scale has begun to fall below the expected value. For $x_1/b_0 > 200$ the length scale variation also starts to become less than expected. This is the sequence of scale variations exhibited in the preliminary arrangements discussed above where the "proper" jet behavior could not be achieved for smaller values of x_1/b_0. The variation in the velocity scale is consistent with the analysis by Schneider (1985) and the consequences of the above approximate analysis. Under severe confinement, distortions in both characteristic jet scales have been reported for axisymmetric jets by So, Ahmed & Yu (1987). Since the total momentum is approximately proportional to $b \times (U_1)^2$, it is clear that the momentum is decreasing as well and this is seen to be the case in Fig. 10a. The figure contains the streamwise momentum flux

variation for jets 1 and 10 as well as that of Vanvari and Chu (1974). The momentum, J, is calculated from

$$J(x_1) = \int_{-\infty}^{0} \left(U_1^2 + \overline{u_1^2} - \overline{u_2^2} \right) dx_2, \tag{9}$$

except for that of Vanvari and Chu who neglect the turbulent normal stresses. We also found that the additional flux due to turbulent fluctuations was a small portion of the total ($< 6\%$) because of their tendency to cancel except near the free surface where $\overline{u_2^2} \rightarrow 0$. All of the curves exhibit an initial development region followed by varying rates of decline. Some of this behavior can be explained with reference to Fig. 5 and noting the apparently favorable hydrostatic pressure gradient in the near-jet field followed by an adverse gradient further downstream. These gradients have not been included in the jet momentum balance due to the belief that they are present to drive the entrained return flow and therefore exist largely in the lower fluid. It is well known, however, that the characteristics of the upstream boundary layer ($x_1 \leq 0$) exert a profound influence on jet development. Hussain and Clark (1977) report increases in total average streamwise momentum of between 20% and 56% within the first 40 slot widths for several sets of initial conditions. The larger increases occur for initially low Re and laminar boundary layers and about 10% of each increase is due to the developing turbulence field. The increases are found to be consistent with gradients in static pressure, however, precise measurements of pressure do not lead to a balancing of the corresponding increases in momentum. As noted by Hussain and Clark, this appears to emphasize that pressure measurements in turbulent flows are subject to yet undetermined influences. The conventionally defined shape factors (δ_1/δ_2) for jets 1 and 10 are 1.19 and 3.41 respectively. The first of these is typical of a constant pressure turbulent boundary layer while the second compares with that calculated for a Falkner-Skan laminar flow boundary layer approaching separation (Reynolds (1974)). Considering these characteristics along with the Reynolds numbers listed in Table 2, jets 1 and 10 are found to behave very similar to those studied by Hussain and Clark insofar as their early development is concerned. In any event, following the transition region, jet 1 exhibits a decline in momentum which resembles the behavior calculated from Eq. (1) if the result is normalized to conditions at $x_1/b_0 = 20$. The relatively good correlation breaks down in the range $80 \leq x_1/b_0 \leq 120$ and the momentum distribution may be said to deviate in excess of 10% from that predicted by Eq. (1) by $x_1/b_0 = 160$. The momentum decay for jet 1 on the other hand, decays logarithmically only in the range $20 \leq x_1/b_0 \leq 40$ and this is followed by a rapid drop. The results of Vanvari and Chu show also a short development region wherein the jet momentum increases to approximately $1.05J_0$ and then rapidly decays. Figure 10b illustrates the mass flux variation for each of the three experiments discussed above and it is apparent that jet 10 has stopped entraining in the vicinity of $x_1/b_0 = 160$. The other experiments show only a very small region in x_1/b_0 wherein the development is free of finite-depth effects.

Table 3 lists the values of the jet spreading constants defined in Eqs. (4-5) together with "consensus" values reported elsewhere for planar surface jets and other geometries. Those listed for the present study are for jet 10 (Figs. 9a-b) only. If all of the

experiments of the present study listed in Table 2 are taken into consideration, we found $0.042 \leq C_1 \leq 0.063$ and $0.048 \leq C_3 \leq 0.065$. As mentioned in the discussion of Figs. 8a-b, there are perceptible Reynolds number effects on the results, however this study has made no effort to define them more clearly. The Reynolds number sensitivities appear to follow those noted separately by Hussain and Clark (1977) and Kotsovinos (1976).

Table 3. Jet Spreading Constants

Configuration/Ref.	C_1	C_2	C_3	C_4
surface jet				
present study	0.047	0.04	0.05	0.9
Rajaratnam (1969)	0.082	—	—	—
Rajaratnam (1984)	0.104	—	0.07	—
Vanvari & Chu (1974)	0.090	—	0.045	—
wall jet				
Rajaratnam (1976)	0.081	—	0.068	—
via Launder & Rodi (1981)	0.062	—	0.073	—
free jet				
Rajaratnam (1976)	0.082	—	0.1	—
via Ramaprian (1985)†	0.093	—	0.095	—
	0.27	—	0.115	—

†(upper and lower bounds of data surveyed)

In the following section, we discuss the evolution of the mean and turbulent velocity fields of jet 10 with particular emphasis on the region near the free surface.

RESULTS AND DISCUSSION

The profiles of the mean longitudinal velocity U_1 are shown in Fig. 11 for the ten measurement stations when scaled by the local maximum, U_{1_m}, and jet half-width, $b(x_1)$. This figure also contains the symbol table relevant to the next several figures to be discussed. The characteristic half-width dimensions were determined as the locations where the mean velocity dropped to one half of its maximum value. The maximum velocity at any stations always occured at or very close to the free surface. The first two measurement stations ($x_1/b_0 \leq 4$) were in the developing region of the jet and exhibit a uniform potential flow above the spreading shear layer emanating from the solid lip of the jet origin. For the remaining measurement stations in the fully developed jet, traditional similarity in the mean velocity profiles is achieved based on these two characteristic scales. Some scatter in the results is found near to the free surface and in the lower portions of each profile particularly at the furthest stations downstream.

Some of the variance in the lower portions is attributable to the rectification of velocity fluctuations which are larger than the local mean at the edge of the jet. The hot-film anemometers cannot differentiate flow direction under these conditions and

therefore indicate a larger mean velocity in proportion to the root-mean-square fluctuations. This is clearest in the third and fourth stations where the profiles never attain zero values deep into the entraining fluid.

The presence of turbulence in the entrained fluid is also further evidence of influence on the results by the finite channel depth. The distortions in the lower portions of the later stations are in the region of the jet where the bottom return flow is approaching the magnitude of the jet flow itself and the expected jet behavior is breaking down as we discussed in the previous section. The results from the preliminary jet series showed similar distortions in the tails of the velocity profiles. However, overall similarity in the mean velocity profiles based on the measured values of U_{1_m} and $b(x_1)$ could always be achieved to the same degree as shown in Fig. 11. Thus, the occurence of such similarity is not a sufficient condition for "proper" jet behavior as has often been claimed in the literature. Apparently, confined jets will exhibit classical similarity when based on the measured characteristic scales. Only momentum considerations as described in the previous section can provide necessary conditions for 'proper' jet behavior.

The scatter in mean velocities near to the surface is largely unexplained beyond the difficulty in maintaining calibrations in that region and the influence of an intrusive measurement near to the surface. For $x_1/b_0 \leq 20$ some of the scatter can be attributed to the steady, free surface wave pattern as indicated in Fig. 5. The mean velocity data shown in Fig. 11 are the averages at each station for the "lower" series of measurements which is to say the sequences that started at the jet lip elevation, moved up toward (but short of) the surface and then stepped down through the jet. These measurements rarely exhibited any trend toward a zero mean velocity gradient at the surface except in the early jet. In contrast, the free surface measurement series which also began at the lip elevation before stepping up in much smaller increments toward and through the free surface did usually exhibit a very narrow zero gradient layer below the surface. Due to the increased density of contaminants near the surface, however, the before-and-after probe calibrations for these measurements often differed widely. As such the velocity data are not as reliable in the lower series of measurements. As the probe began to deform and to eventually break through the surface, the indicated velocity would monotonically decrease to a value representing convective and evaporative heat losses in air. There was no sharp delineation in the mean velocity measurement associated with the interface. The results presented in the most of the following figures are based on the averages of the lower measurement series. The upper series were used in estimations of turbulent scales and spectra which are discussed in the later sections.

The vertical profiles of the three turbulent intensity distributions are shown in Figs. 12a-c where the symbols follow the table given in Fig. 11. These distributions serve to illustrate some of the principal structural characteristics that differentiate the surface jet from either the free jet or the wall jet. In the fully developed free jet there are clearly defined local minima in $\overline{u_1}$ and $\overline{u_3}$ in the symmetry plane since there is negligible turbulence production in this region. The vertical fluctuation, on the other hand, being closely correlated (negatively) with the static pressure distribution is found

to be at a maximum in the symmetry plane. In the wall region of a wall jet, of course, all velocities approach zero. Due to scatter, the current data are inconclusive as to the precise structure of the horizontal components very near to the surface. At the downstream stations the distributions of these components appear to reach a local minimum near the surface but in a small region very near the surface there is a tendency for the horizontal components to increase in magnitude. These measurements, however, may be influenced by surface blockage and sporadic encounters with contaminants. The vertical component, however, shows a clear tendency toward vanishing near the surface. Except for the developing region of the jet ($x_1/b_0 \leq 4$) the distributions shown in Figs. 12a-c also ought to exhibit similarity when non-dimensionalized with U_{1_m} and $b(x_1)$ according to classical notions of a free jet. Wall jets have an outer and an inner length scale in order to account for the wall boundary layer. The one length scale similarity of the surface jet profiles is inadequate near to the surface. In a relative sense there is progressively more turbulent kinetic energy in the two horizontal components ($\overline{u_1}, \overline{u_3}$) as x_1/b_0 increases while the vertical component ($\overline{u_2}$) remains about the same. This is the trend exhibited in the longitudinal traverses shown in Fig. 6. Also evident is the growing anisotropy between the three turbulence components with distance downstream and proximity to the surface. These trends are examined in greater detail in the following paragraphs.

Figure 13 illustrates these turbulence distributions using the local profile maximum intensity to normalize the data. Better collapse of the overall profiles is obtained in this way and it serves to reveal the scatter in the turbulent intensities near to the surface for the two lateral components versus the better precision in the profiles for the vertical fluctuation. This was a feature of all of the measurements for both the lower and upper measurement series. We believe this is due to a lack of overall stationarity in the data due to the large scale structures originating at the jet lip. Dye injection in this region revealed the regular but low frequency production of laterally-oriented vortices. Turbulent diffusion of the dye prevented the visual observation of these structures further downstream. At the far downstream stations these structures must pass the measuring point at a considerably lower frequency due to the decay in the convection velocity and it is probable that the sampling frequencies and sampling times listed in Table 1 were not fully adequate in this region. The data suggest that the structures are contracting vertically, hence expanding longitudinally, near the free surface since the vertical component is relatively free of the low frequency (large scale) fluctuation.

The measured turbulent shear stress distributions are plotted in Figs. 14a-b using both the traditional velocity scale and the local maximum, respectively, to assist in identifying particular locations of large variances in the data. In this instance, the conventional velocity scale is adequate within the experimental accuracy and no particular trends are evident. The fluctuating shear stress is rapidly nearing zero as the free surface is approached but may have a non-zero value at the surface. This is consistent with the presence of surface contamination which would support a fluctuating shear. The correlation of these velocity components under linear capillary waves is zero and not expected to contribute to the measurement. The longitudinal variations of the three normal turbulent stresses, $\overline{u_i^2}/U_{1_m}^2$, are shown in Figs. 15a-c. These plots were

obtained by taking the maximum value in the corresponding profile. For the vertical fluctuations and the upstream profiles of the other two components the maximum always occurred well below the surface within the center of the jet. As the jet develops downstream the vertical profiles of the longitudinal and lateral componenets become more uniform in the region between the free surface and the central portion of the jet so that the maximum in the profile eventually is found at or near to the surface. The data in Figs. 15a-c represent the respective maximum values regardless of x_2-location. It is clear from Figs. 12 and 13, however, that the free surface magnitudes of $\overline{u_1}$ and $\overline{u_3}$ at the downstream stations are similar to the magnitudes lower in the jet where the maximum values for a free plane jet would occur.

The longitudinal variations of $\overline{u_i^2}/U_{1_m}^2$ exhibit the classical rapid growth and perhaps overshoot in the developing segment of the jet before settling into an asymptotic far field behavior. Typical asymptotic behavior for plane free jets [c.f. Ramaprian & Chandrasekhara (1985)] reveal constant values of $\overline{u_1^2}/U_{1_m}^2$ and $\overline{u_2^2}/U_{1_m}^2$ in the farfield on the order of 0.06 and 0.04, respectively. In the present case of the surface jet, the longitudinal component maximum does not achieve a constant asymptote but continues to amplify downstream in reflection of a redistribution of turbulent kinetic energy. The lateral component exhibits an apparent asymptote of approximately 0.017 before beginning to increase for $x_1/b_0 > 160$. The evolution shown for the $\overline{u_2^2}/U_{1_m}^2$ component is entirely within the body of the jet and compares very well with classical results for other jet geometries. The total turbulent kinetic energy if represented by the sum of these contributions also appears to grow with distance downstream but it must be recalled that these maxima do not always occur at the same elevation within the jet. The asymptotic behavior for the turbulent shear stress is shown in Fig. 16. An asymptote on the order of 0.01is achieved as compared to values around 0.025 for free plane jets.

In order to gain insight into the structure of the turbulence near to the free surface, estimates were obtained of the one-dimensional spectra along with the turbulent macroscales, L_i, and microscales, λ_i. Turbulent frequency spectrum estimates were computed from ensemble averages of FFT results for all blocks of time series data. The first pass used all of the data in one block and the second pass took every other point from two blocks in order to resolve a greater range of time scales. Using Taylor's frozen turbulence hypothesis these spectral estimates were converted to wavenumber spectra in the classical manner ($k = 2\pi f/U$) using the local value of $U_1(x_2)$. The turbulent microscale was estimated from the spectra using

$$\lambda_i = \left(2\overline{u_i^2}\right)^{\frac{1}{2}} \left(\int_0^\infty F_i(k)k^2 dk\right)^{-\frac{1}{2}}, \tag{10}$$

where in this case the wavenumber function satisfies,

$$\int_0^\infty F_i(k)dk = \overline{u_i^2}. \tag{11}$$

These scale estimates are shown in Figs. 17a-c where the numbers used to plot the data points represent the relative elevation in the surface measurement series. The numbers increase with distance from the free surface in uniform increments of 0.18 *cm* with '0' representing the nominal free surface and elevation '4' representing the elevation of the jet lip. Elevation numbers greater than five correspond to locations in the body of the jet taken in the "lower" measurement series. These are plotted only for the longitudinal microscale for comparison. The local free surface elevation varied somewhat from the nominal datum as indicated by Fig. 5. The local uncertainty in the mean water level datum is typically 0.05 *cm* which was a result of the surface wave fluctuations in general and the interactions of the upper probe support with the unsteady free surface as it broached above the sensing elements. The variances in the data are too large with respect to apparent trends in the results to extract the influence, if any, of the free surface upon the microscale estimates. This is consistent with the spectral behavior over a range of wavenumbers to be discussed later in this section.

The macroscale estimates were obtained via the autocorrelation function,

$$R_{ii} \equiv \overline{u_i(t)u_i(t+\tau)}/\overline{u_i^2},$$

and

$$L_i = U_1 \int_0^\infty R_{ii}(\tau)d\tau, \tag{12}$$

where Taylor's hypothesis is again assumed. The results are plotted in Figs. 18a-c where the numbering of data points is as described in the discussion of Figs. 17a-c above. The dimensional variation of the jet half-width scale, $b(x_1)$, is included in the figure and a straight line has been drawn through that data for comparison to the macroscale estimates. In the longitudinal direction, the macroscale is of about the same magnitude as $b(x_1)$ and varies in like manner as one might expect. Also typical for shear flows the lateral scale L_3 in Fig. 18c grows with distance downstream but is some fraction of order 1/2 of the longitudinal scale. There is a suggestion that proximity to the surface (smaller elevation numbers) reduces this scale as well but the data is ambiguous. The vertical turbulent macroscale, L_2, is clearly influenced by the free surface to the extent that much of the downstream development is suppressed and nearly uniform scale estimates are obtained in the upper half centimeter or so (points 0-3). The apparent onset of longitudinal developments in this scale between elevation numbers 3 and 4 ($0.58\ cm < x_2 < 0.76\ cm$) is noteworthy. At this elevation and in this probe orientation the upper probe support is approximately 0.13 *cm* above the sensing elements and therefore at least 0.45 *cm* from the nominal mean free surface elevation. It is too deep to envision a probe intrusion effect that would not also contaminate any conventional uses of the probe. Thus the observed trend is a surface effect upon the turbulent structure whereby the vertical scale of the fluctuations is suppressed very rapidly in a narrow layer close to the surface. Variations in the affected vertical macroscale within the surface layer are not resolved by these estimates.

Vertically spaced sequences of typical turbulence spectra are plotted in Figs. 19 through 26 representing each of the measuring stations along the fully developed jet. The top four spectra in each stack were obtained from the upper measurement series and correspond to the data symbols 1 through 4 in the previous few figures. The bottom spectrum in each stack is obtained at mid-depth location ($x_2 = b(x_1)$) for comparison to the surface influenced layer. Within each plot the symbols '1', '2' and '3' denote the three component directions. The large uncertainties at the smallest wavenumbers stem from the inability to maintain stable calibrations of the probes over sufficiently long measurement durations. Hence the scatter at these wavenumbers is the result of very low frequency fluctuations in the jet combined with drifts in the sensor calibrations. The two processes are indistinguishable in the data and it is not possible to draw conclusions on the exact shape of the spectra in the lowest wavenumber range. All of the spectra were integrated to insure that the total turbulent energy matched the earlier computations of $\overline{u_i}/U_{1_m}$. The axes scales for all of the spectra are identical to facilitate comparisons.

The downstream development of the jet away from the surface is best illustrated by comparing the sequence beginning at the bottom spectra of each stack ($x_2 = b(x_1)$). For most of the wavenumber range ($k \geq 5$) the three components of turbulent fluctuations are about the same in consequence of isotropy. As the jet develops downstream the spectra at depth evolve into the classical shape containing isotropic equilibrium and dissipation ranges with distinguishable and appropriate slopes in each range on the log-log plots. At the lowest wavenumbers the spectra exhibit anisotropy with greater energy in the longitudinal components as would be expected for this type of shear flow. The energy content of vertical and lateral components are approximately equal throughout this development.

Within the upper layer of the fluid the following trends become apparent. As the jet develops downstream a separation between the lateral and vertical spectra grows. More energy is found in the low wavenumbers of the lateral components, 3, at the expense of the vertical components, 2, as compared to the spectra below ($x_2 = b(x_1)$). Eventually the lateral components approach the distribution of the longitudinal components. This behavior is comparable to the theoretical results of Hunt & Graham (1978) for the moving wall problem. However, that theory predicts a flat cut-off in the low wavenumber region of $(\overline{u_2}/U_{1_m})^2$ beginning at a wavenumber corresponding to 1/4 of the distance from the wall (interface). The spectra measured here for the free surface jet contain significantly increasing energy in the vertical direction as the wavenumber is reduced and any variation in the cut-off wavenumber with distance from the surface does not match either the linear form or the magnitudes predicted by the theory. The cut-off wavenumber does appear to increase as the surface is approached in most of the vertical stacks, however, the most appropriate variation seems to be linear on these plots as shown for example in Figs. 25 and 26. Given that the wavenumber axis is logarithmic, the variation of cut-off wavenumber with distance from the surface cannot be linear.

The additional energy in the vertical component above a flat spectral level cut-off for wavenumbers less than the cut-off could be attributable to the surface wave

fluctuations. Very small wave amplitudes on the order of those in the later stages of the jet ($\sim 0.05\ cm$) could give rise to apparent turbulent fluctuations of the magnitudes observed here. However, these ought to be greatly attenuated with depth in this range and equally evident in each of the two lateral components assuming omnidirectional propagation of the waves. The proper depth attenuation is not evident in the data and the magnitudes of the two lateral components do not appear sufficiently larger than the $x_2 = b(x_1)$ distributions to contain an equal amount of wave fluctuation energy implied by the increase in the vertical component over a flat distribution. One must be careful to note the nearly order of magnitude difference between energy levels of the vertical fluctuations and the levels of the two horizontal components. It appears that the increase in $(\overline{u_2}/U_{1m})^2$ with decreasing wavenumber is a feature of the surface-influenced turbulent layer which is not captured by the moving wall theory. This may be a consequence of interactions between the intermediate turbulent scales near to the surface which are not contained in the theory as noted by Hunt & Graham (1978).

The overall balance of turbulent kinetic energy is difficult to deduce with accuracy from the data. At first glance the two horizontal components of turbulence appear unaffected by the presence of the surface while the vertical component is significantly attenuated below the cut-off wavenumber which produces the anisotropy. This suggests a decrease in total turbulent kinetic energy approaching the surface which is consistent with the moving wall theory of Hunt and limited experiments. The theory and moving wall measurements indicate a recovery toward the farfield value of total turbulent kinetic as the wall is reached but the present measurements do not display this recovery. All or most of the lost turbulent energy may have been expended in the generation of vertical surface motions which are then radiated away as waves. Coupled velocity, pressure and surface motion measurements are needed to resolve this energy balance fully. An more complex balance is suggested by a comparison of affected turbulent scales in the following paragraph.

The various scales at which anisotropy between components are observed from the spectra are plotted in Fig. 27. For reference, the scale corresponding to anisotropy at $x_2 = b(x_1)$ in the body of the jet is plotted as the crosses in the figure. Typically, this scale corresponds to the wavenumber where both the vertical and lateral components begin to diverge from the longitudinal component. This scale grows approximately linearly along the jet as one might expect for a shear flow of this nature and is not influenced by the presence of the surface. The solid circles represent the average scale at which the longitudinal and lateral components begin to diverge under the influence of the free surface. Clearly, the free surface has caused these two components to become comparable at much larger scales (smaller wavenumbers) than in the body of the jet by an amount that grows with distance downstream. In other words the free surface has rendered the lateral turbulent motions nearly indistinguishable for all but perhaps the largest scales. The bars on each data point cover the range of values found in the surface-influenced layer.

The average scale corresponding to the cut-off wavenumber for the vertical fluctuations is plotted as the open circles in the figure and the range of values is again

indicated by the bars on each point. In this case the influence of the surface layer is to decrease the scale at which the vertical component remains comparable to the other two. In other words the free surface acts to suppress these fluctuations and therefore increases the difference. This is the trend indicated by the spectra. This scale approaches the microscale by eliminating the equilibrium range for the vertical fluctuations but does not quite reach that value which is consistent with the microscale estimates obtained earlier from these spectra. These cut-off scales are approximately the distance of the measurement point from the surface on average. Taken together the scales suggest that the energy balance includes a redistribution of the vertical turbulent energy into at least the lateral fluctuations as well as the generation of surface waves. This is consistent with all of the data presented here but the exact nature of the energy redistribution must await further analysis and concommittant measurement of the radiated wave field.

SUMMARY AND CONCLUSIONS

The results of the this investigation into the behavior of free surface jets are applicable to the synoptic characteristics of this and similar jet configurations as well as the influence of a free surface on the nearby turbulent flow. The synoptic or global surface jet behavior is similar to that of a wall jet at comparable Reynolds numbers and inlet conditions. The effects of jet confinement are pervasive and subtle to the point where considerable doubt exists about many results reported in the literature. The results of an approximate analysis to account for facility constraints is shown to correlate well with departures from anticipitated scale behaviors for the current experiments as well as others. Mean velocity profile similarity is observed at the furthest downstream stations investigated and after the jet development is significantly influenced by the limited depth. The jet momentum variation, however, remains as a primary indicator of the breakdown in jet development. Similar to prior studies of free and wall jets the results of these experiments indicate that inlet conditions will have significant impact on growth rates and momentum variation in the near-origin developmental region. Some Reynolds number trends were noted but more definitive experiments are necessary to further quantify these effects.

At various depths below the free surface, estimates were obtained of the turbulent length scales through the use of one-dimensional frequency spectra and Taylor's hypothesis. The vertical turbulent macroscale is clearly influenced by the free surface to the extent that much of the downstream development is suppressed and nearly uniform scale estimates are obtained in the surface layer. Beginning at moderate values of x_1/b_0 and in the surface layer more energy is found at low wavenumbers in the $\overline{u_3}$ component relative to that in the $\overline{u_2}$ component at these wavenumbers when compared to the relative energy distribution deeper in the fluid. This is consistent with the theoretical results of Hunt & Graham (1978) for the moving wall problem, however, the current data do not exhibit the theoretical prediction of a flat cut-off near the surface in the low wavenumber regime of the $\overline{u_2}$ spectrum. Near the surface the scale at which anisotropy is first observed in the two horizontal components becomes larger with distance downstream and the scale at which the vertical component becomes comparable

to the other two decreases. The data suggest that the energy balance includes at least a redistribution of the vertical turbulent energy into the lateral component.

Additional experiments with a non-intrusive measurement technique and simultaneous measurment of the radiated wave field must be undertaken to permit a more detailed analysis of the energy balance in the near surface region.

ACKNOWLEDGEMENTS

The authors acknowledge the support of the Naval Research Laboratory. One author (M.P.) wishes to acknowledge the support of the ASEE/ONR Summer Graduate Fellow Program which supported him during his stay at NRL. The assistance of Mary Barber in the reduction of the data is also appreciated.

REFERENCES

Biringen, S. & W. C. Reynolds (1981), "Large eddy simulations of the shear free turbulent boundary layer", JFM, 103, 53-63.

Brumley, B. H. & G. H. Jirka (1987), "Near-surface turbulence in a grid-stirred tank", JFM, 183, 235-263.

Chu, V. H. & R. E. Baddour (1984), "Turbulent gravity stratified shear flows", JFM, 138, 353-370.

Goldschmidt, V. & Eskinazi, S. (1966), "Two phase turbulent flow in a plane jet", Trans. ASME, Series E, J. Appl. Mech., 32, 735-747.

Guitton, D. E, (1970), "Some Contributions to the Study of Equilibrium and Non-Equilibrium Wall Jets Over Curved Surfaces", Ph.D. Thesis. Mech. Eng. Dept., McGill University, Montreal, Canada.

Heskestad, G. (1965), "Hot wire measurments in a plane turbulent jet", Trans. ASME. Series E, J. Appl. Mech., 32, 721-734.

Hubbard, D. W., G. Trevino & E. J. Hine (1985), "Experimental Techniques For Measuring Turbulent Velocity Correlations In a Jet Flow Near An Air-Water Interface", Preprints-22, 22nd Annual Technical Meeting, Society of Engineering Science, Pennsylvania State University.

Hunt, J. C. R. (1984), "Turbulence structure in thermal convection and shear free boundary layers", JFM, 138, 161-184.

Hunt, J. C. R. & J. M. R. Graham (1978), "Free stream turbulence near plane boundaries", JFM, 84, 209-235.

Hussain, A. K. M. F. & A. R. Clark (1977), "Upstream influence on the near field of a plane turbulent jet", Phys. Fluids, Vol. 20, No. 9, 1416-1426.

Kotsovinos, N. E. (1975), "A Study of the entrainment and turbulence in a plane turbulent jet", W. M. Keck Lab. Hydraul. Water Resources, Cal. Inst. Tech. Rep., KH R-32.

Kotsovinos, N. E. (1976), "A note on the spreading rate and virtual origin of a plane turbulent jet", JFM, 77, 305-311.

Kotsovinos, N. E. (1978), "A note on the conservation of the axial momentum of a turbulent jet", JFM, 87, 55-63.

Launder, B. E. & W. Rodi (1981),"The Turbulent Wall Jet",*Progress in the Aerospace Sciences*, Vol. 19, 81-128, Pergamon Press, Ltd.

Levich, V. G. (1962), *Physico-Chemical Hydrodynamics* Prentice Hall.

McDougall, T. J. (1979), "Measurements of turbulence in a zero mean shear mixed layer", JFM, 94, 409-431.

Miller, D. R. & E. W. Comings (1957), "Static pressure distribution in the free turbulent jet", JFM, 3, 1-16.

Patel, R. P. & B. G. Newman (1961), "Self-Preserving Two-Dimensional Turbulent Jets and Wall Jets in a Moving Stream", Rep. No. Ae5, Mechanical Engineering Department, McGill University, Montreal, Canada.

Phillips, O. M. (1969), *Dynamics of the Upper Ocean* , Cambridge University Press.

Rajaratnam, N. (1969), "Diffusion of a Supercritical Stream on a Stagnant Pool", Trans. Engr. Inst. Can., Vol. 12, No. A-1.

Rajaratnam, N. (1976), *Turbulent Jets*, Elsevier Scientific Publishing Co., New York.

Rajaratnam, N. & J. A. Humphries (1984), "Turbulent non-buoyant surface jets", Can. J. Hydraulic Res. Vol. 22, No. 2, 103-114.

Ramaprian, B. R. & M. S. Chandrasekhara (1985), "LDA Measurements in Plane Turbulent Jets", ASME J. Fluids Eng., Vol. 107, 264-271.

Ramberg, S. E. & Y. T. Fung (1982), "A New Stratified Towing Channel at NRL", NRL Memorandum Report 4829, Naval Research Laboratory, Washington, D.C.

Reynolds, A. J. (1974), *Turbulent Flows in Engineering*, John Wiley & Sons, New York, 404-405.

Schneider, W. (1985), "Decay of momentum flux in submerged jets", JFM, 154, 91-110.

Shlien, D. J. (1987), "Observations of dispersion of entrained fluid in the self-preserving region of a turbulent jet", JFM, 183, 163-173.

So, R. M. C., S. A. Ahmed & M. H. Yu (1987), "The near field behavior of turbulent gas jets in a long confinement", Exp. Fluids, 5, 2-10.

Tailland, A. & J. Mathieu (1967), "Jet Pariétal", Journal dep1706Mecani[illegible], 6, No. 103.

Thomas, S. M. & P. E. Hancock (1977), "Grid turbulence near a moving wall", JFM, 83, 481-496.

Vanvari, M. R., & V. H. Chu (1974),"Two-Dimensional Turbulent Surface Jets of Low Richardson Number", Fluid Mechanics Laboratory, Technical Report No. 74-2[FML], Department of Civil Engineering and Applied Mechanics, McGill University, Montreal, Canada.

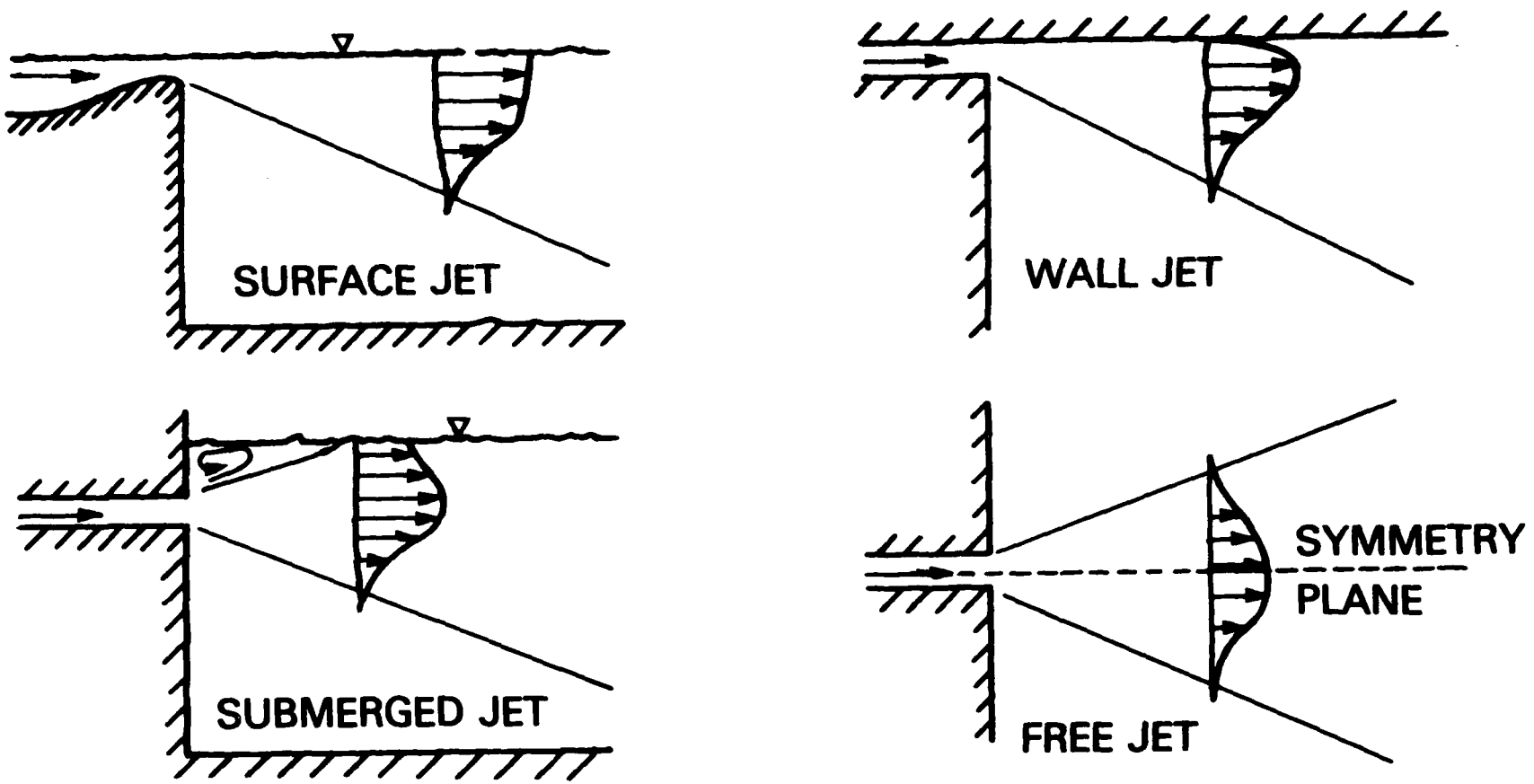

Fig. 1 – Schematic of jet geometries.

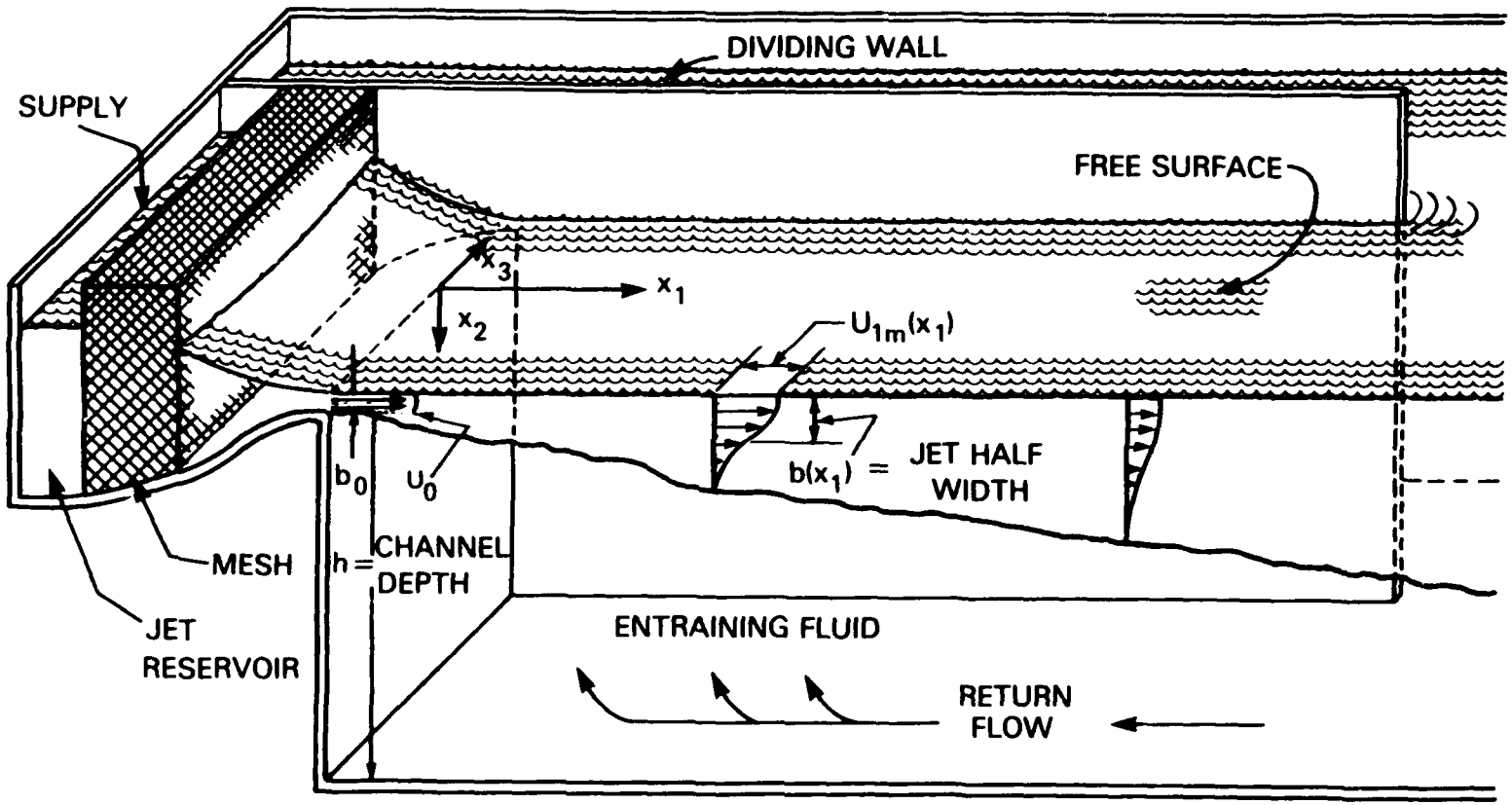

Fig. 2 – Schematic of experimental arrangement showing nomenclature.

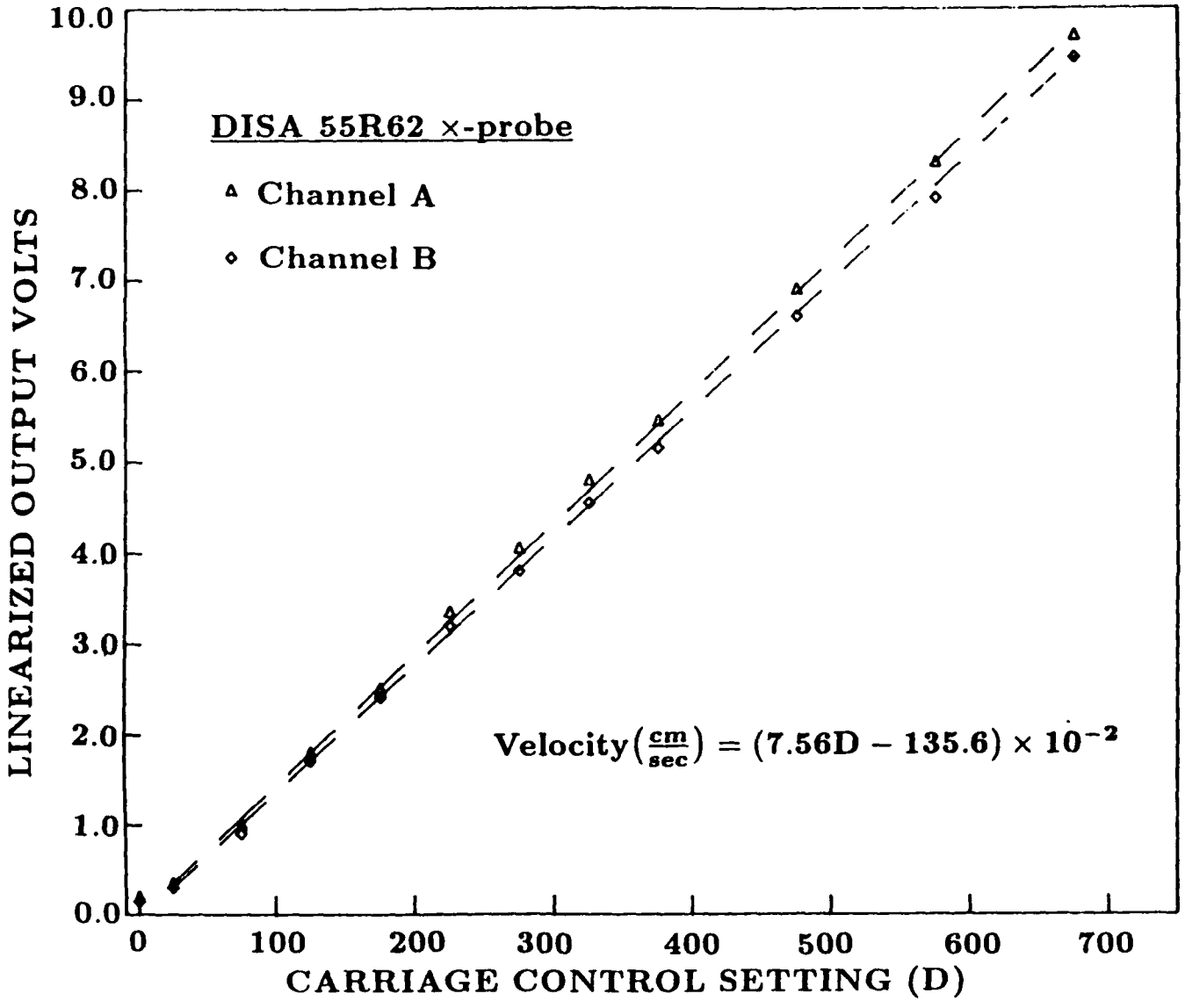

Fig. 3 – Typical calibration curves for cross-film probe.

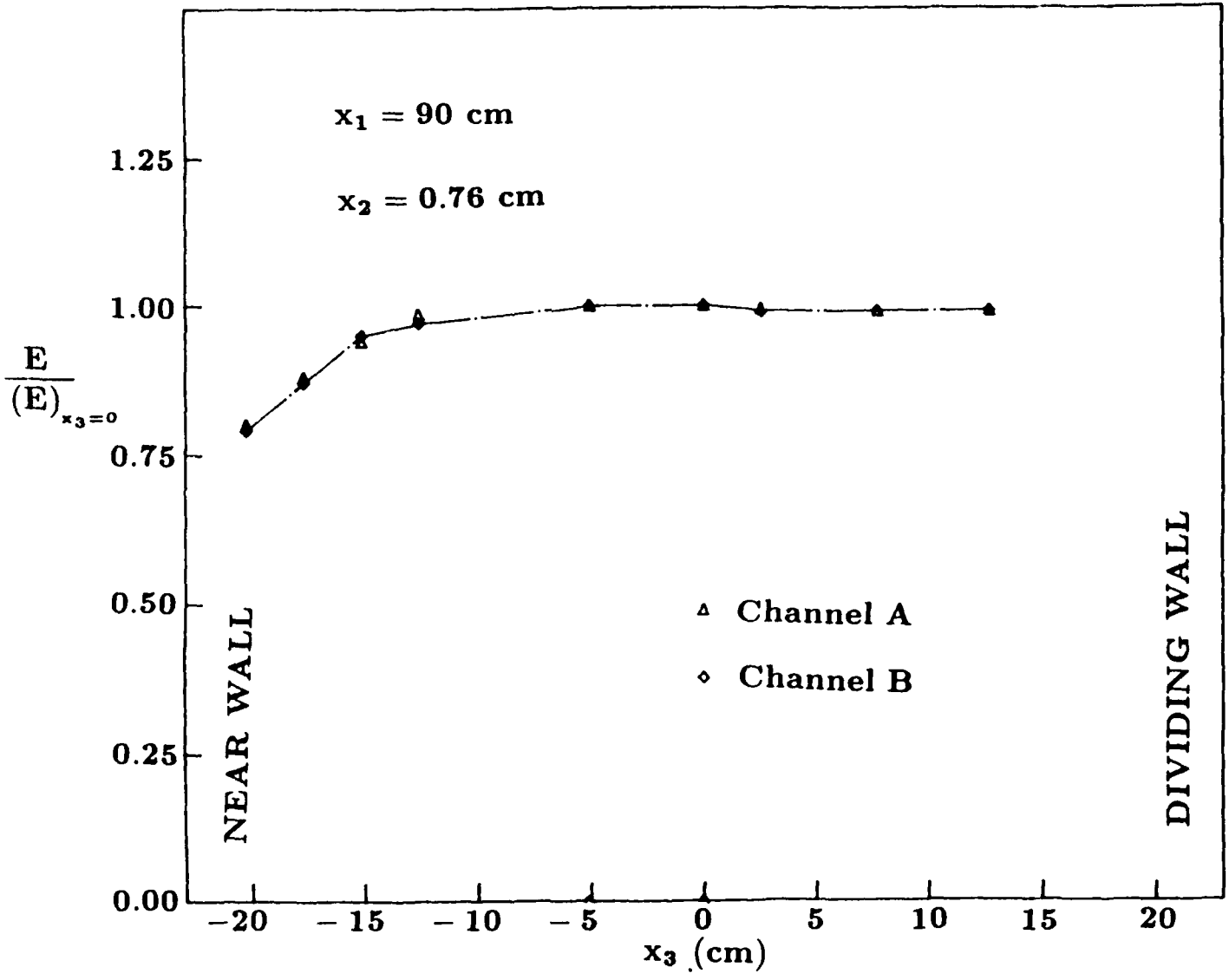

Fig. 4 – Typical lateral variation of output voltages across test section.

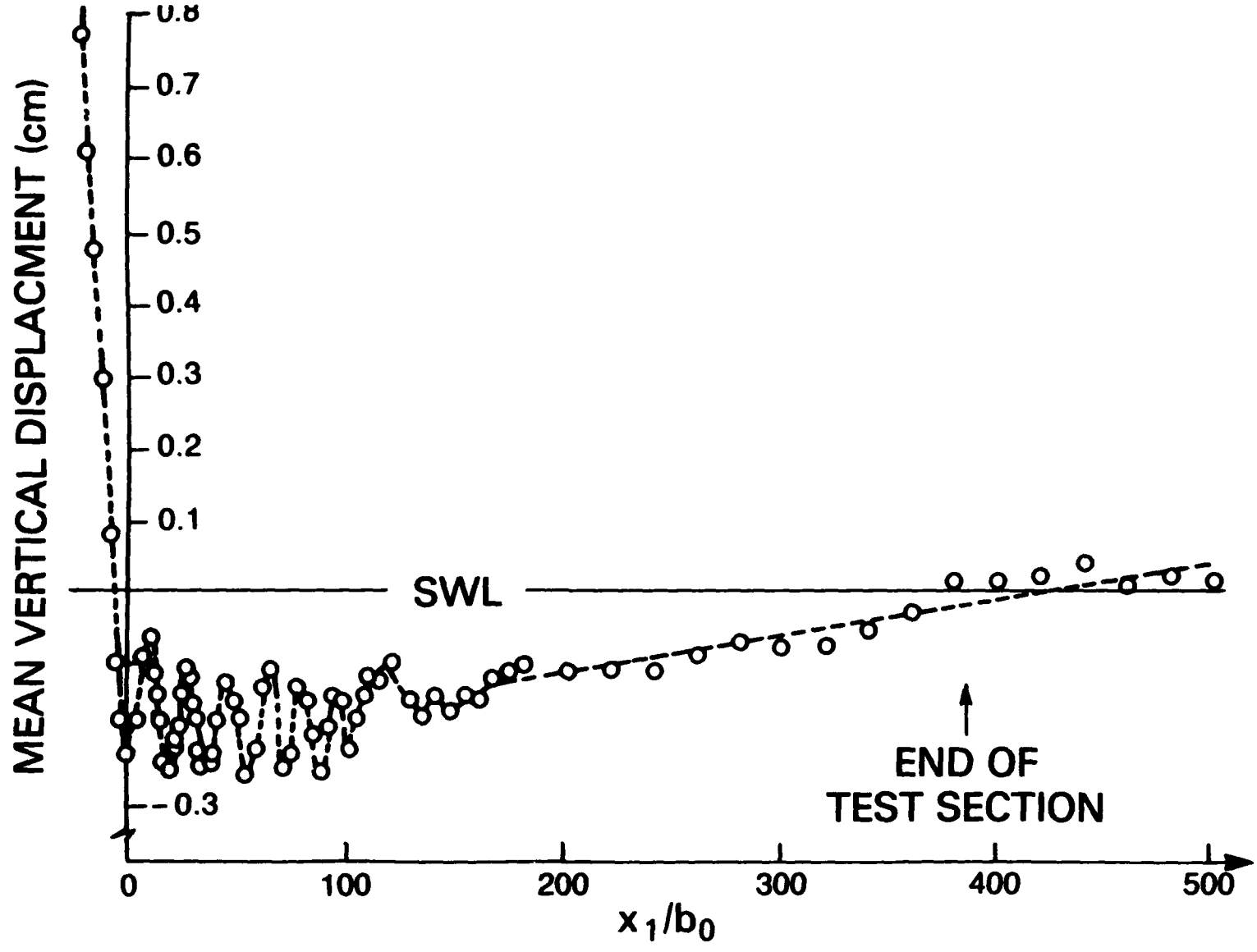

Fig. 5 – Longitudinal variation of free surface elevation above jet.

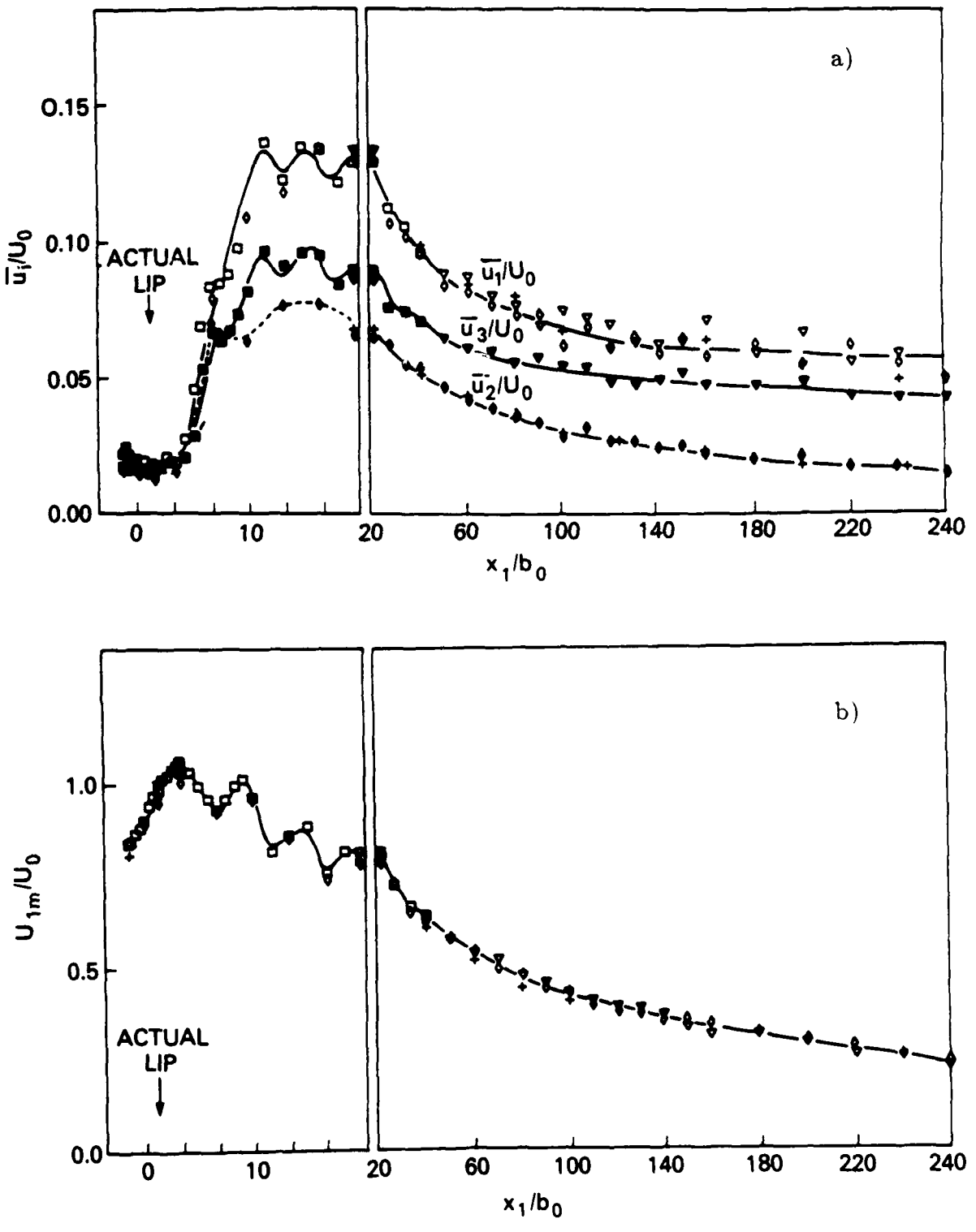

Fig. 6 – Longitudinal variations of a) mean velocity and, b) turbulent intensities below the surface of the jet.

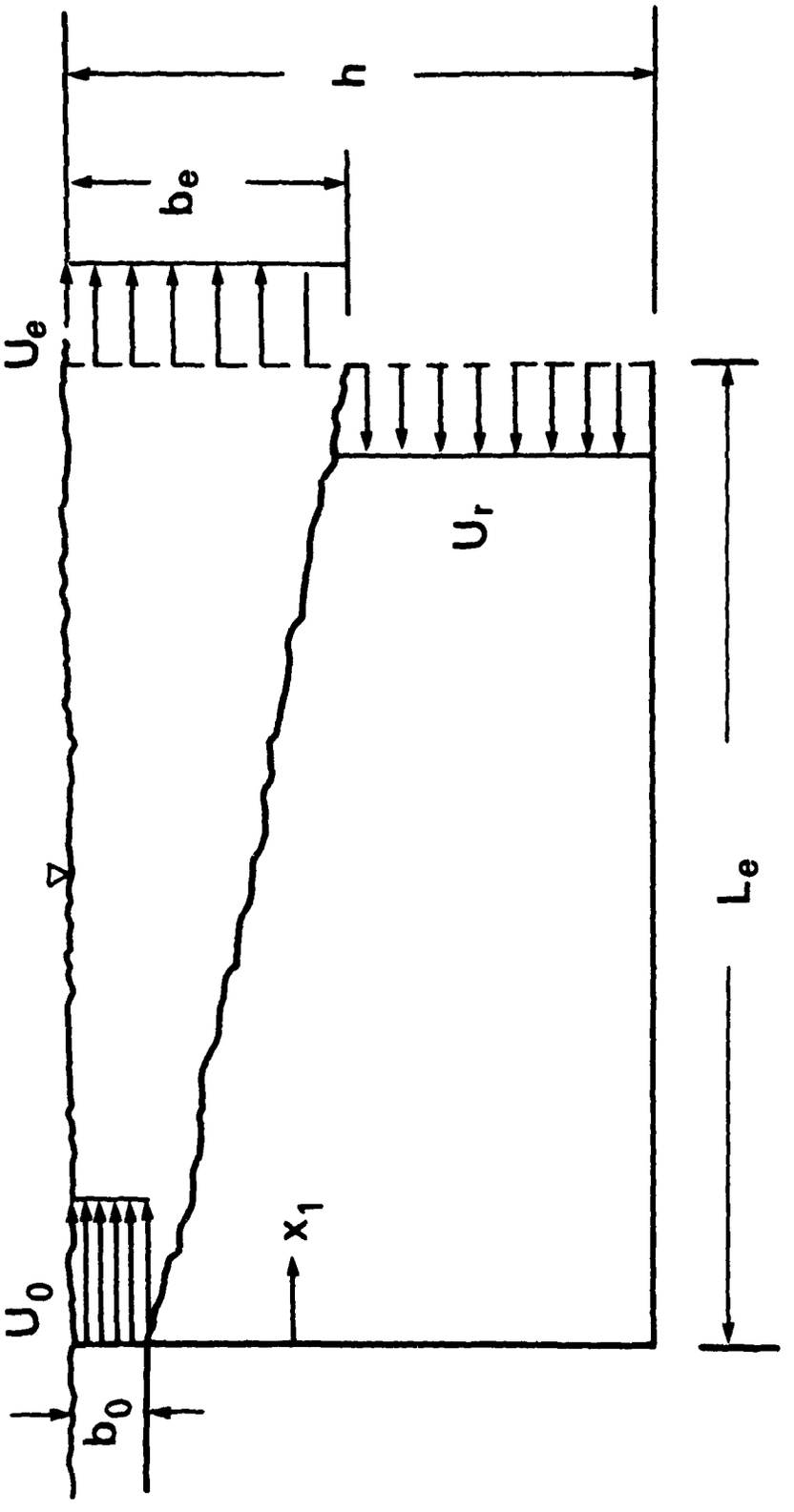

Fig. 7 – Control volume for mass and momentum balances.

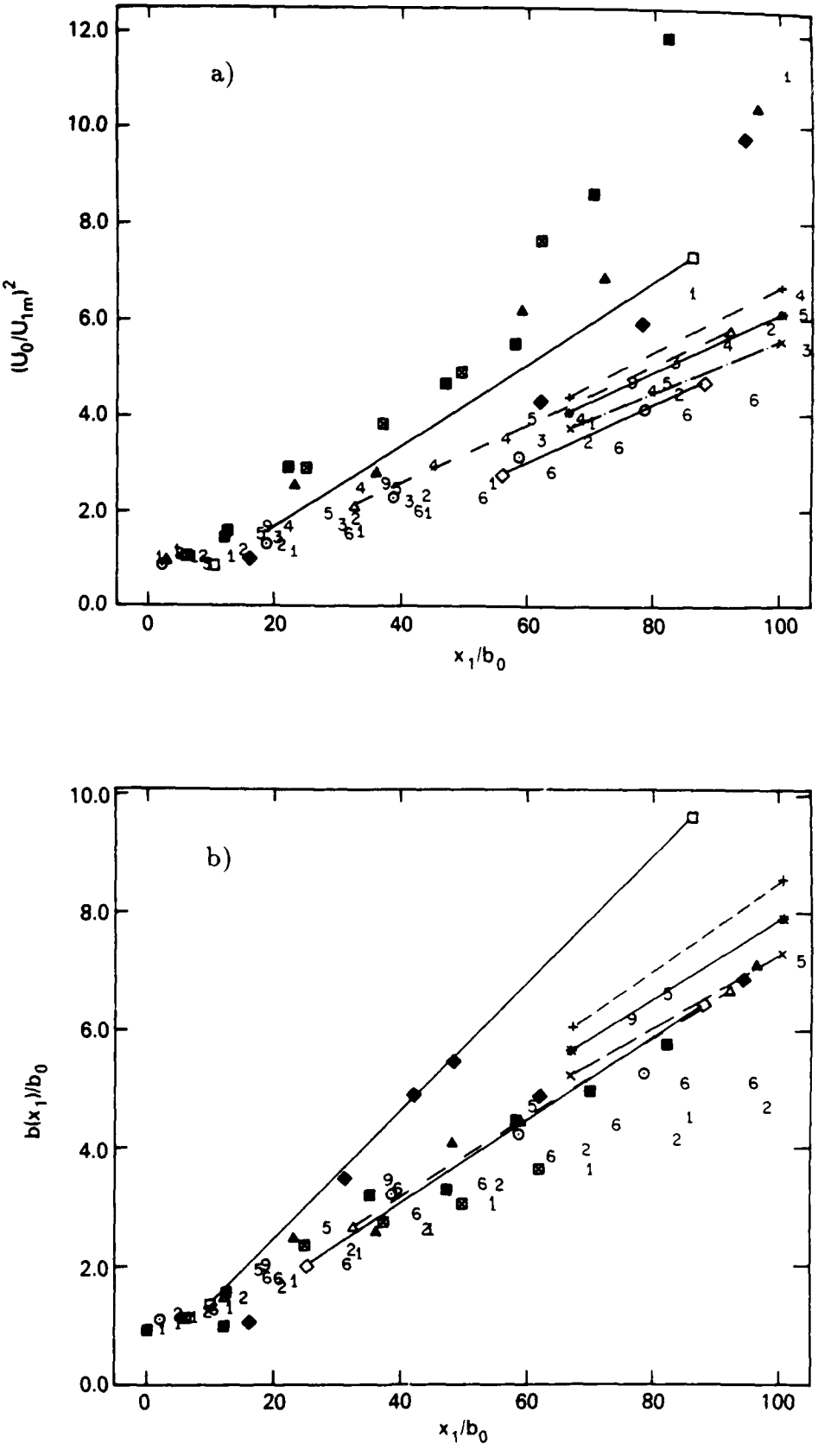

Fig. 8 – Longitudinal variations of a) maximum jet velocity and, b) jet half-width for preliminary experiments.

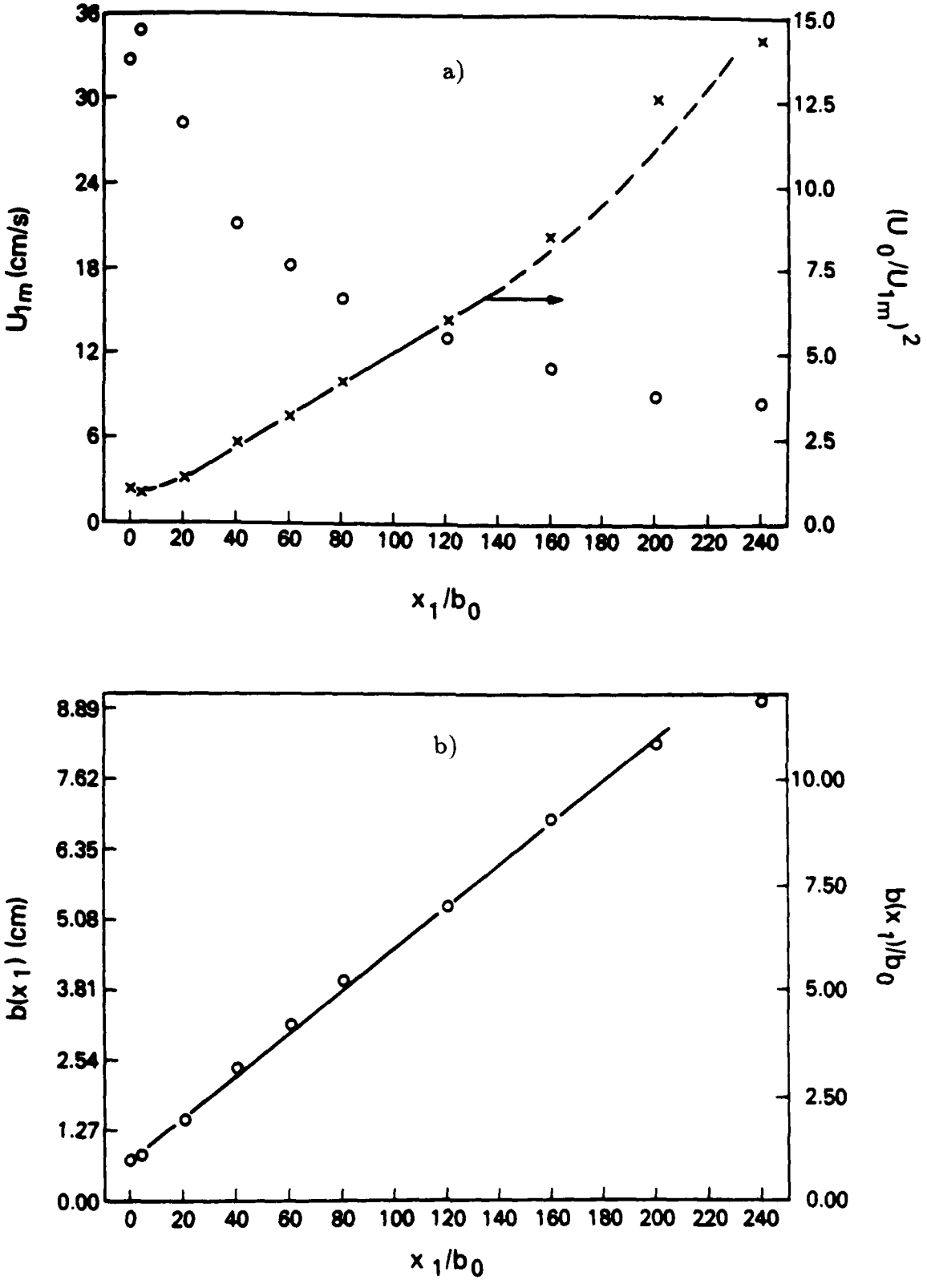

Fig. 9 – Global jet development showing longitudinal variations of the two principal scales; a) maximum velocity. b) jet half-width.

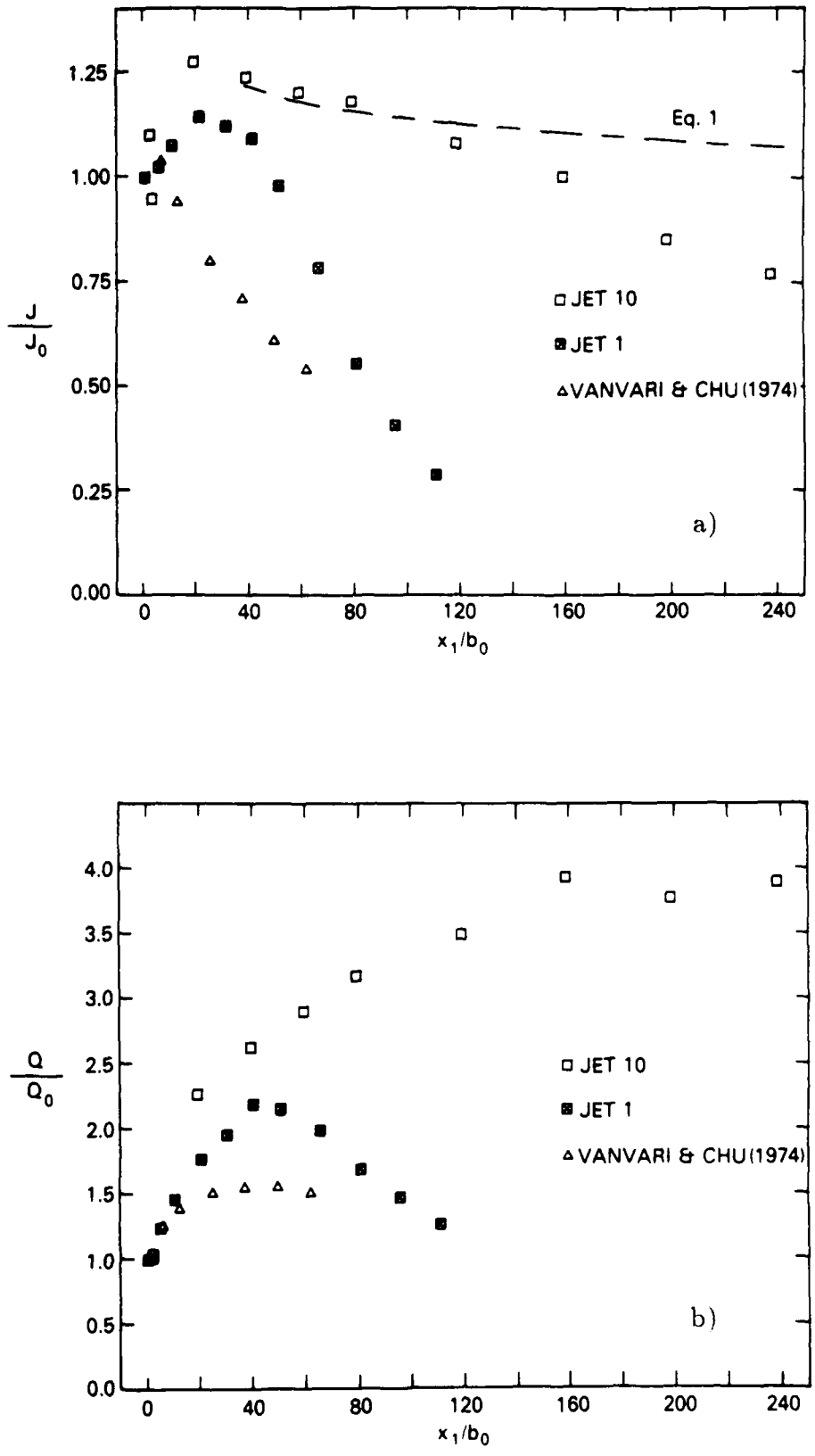

Fig. 10 – Longitudinal variations of a) momentum and, b) mass flux.

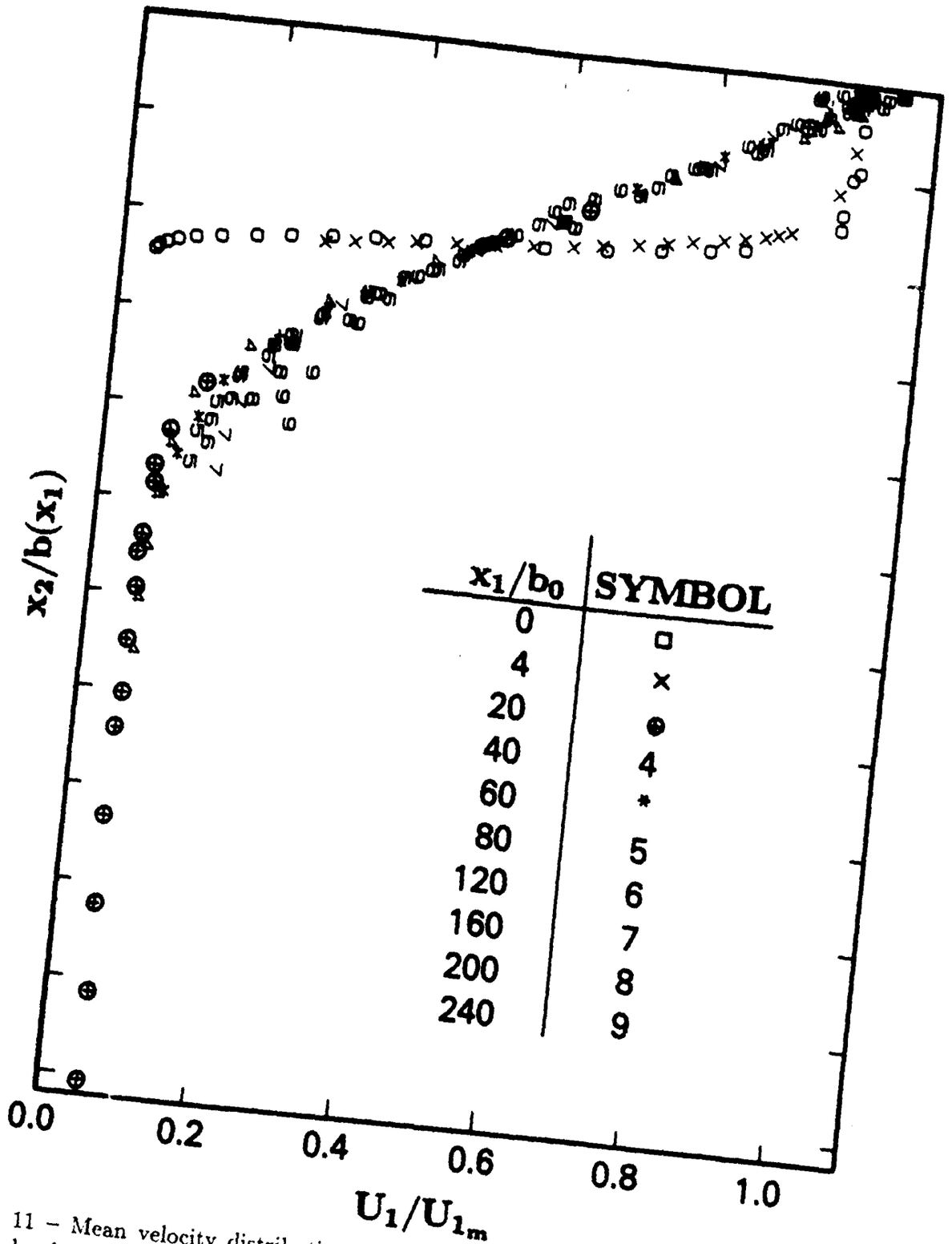

Fig. 11 – Mean velocity distributions at longitudinal measurement stations for the developing jet.

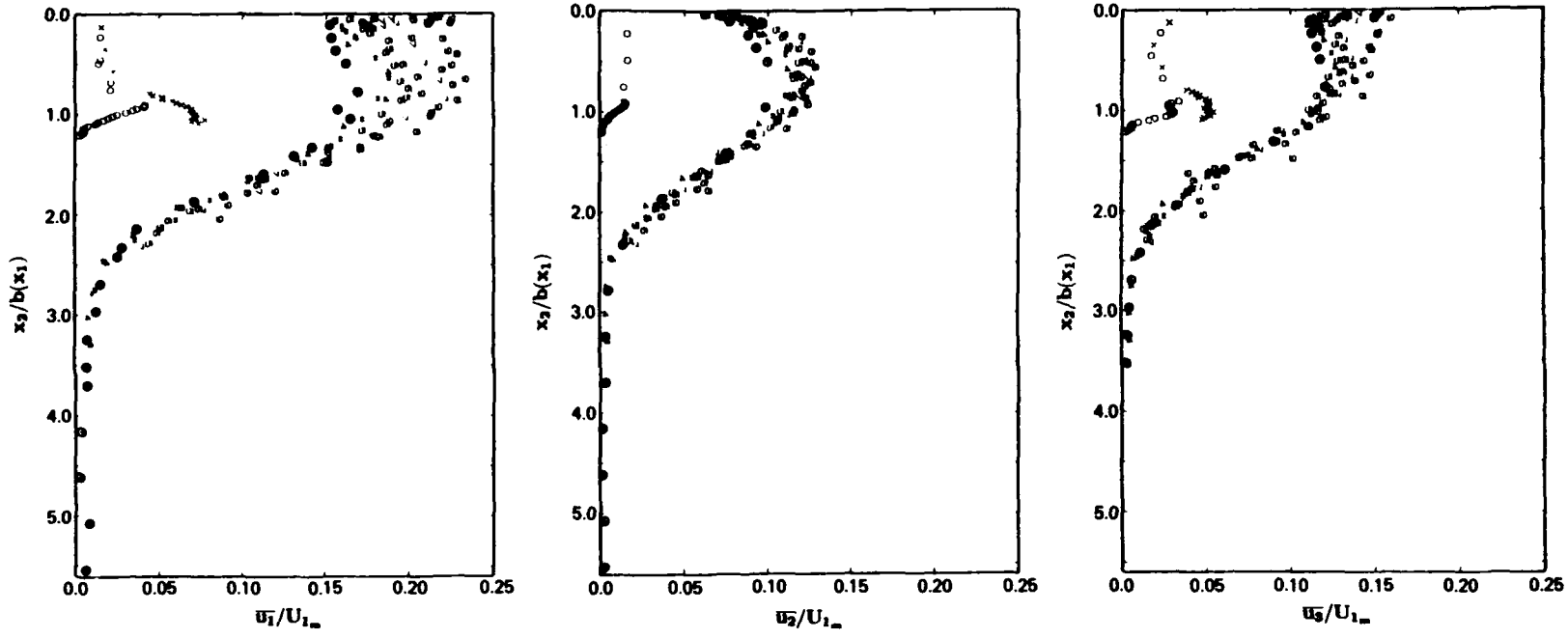

a) longitudinal b) vertical c) lateral

Fig. 12 – Turbulent intensity distributions at longitudinal measurement stations for the developing jet normalized by the mean velocity scale.

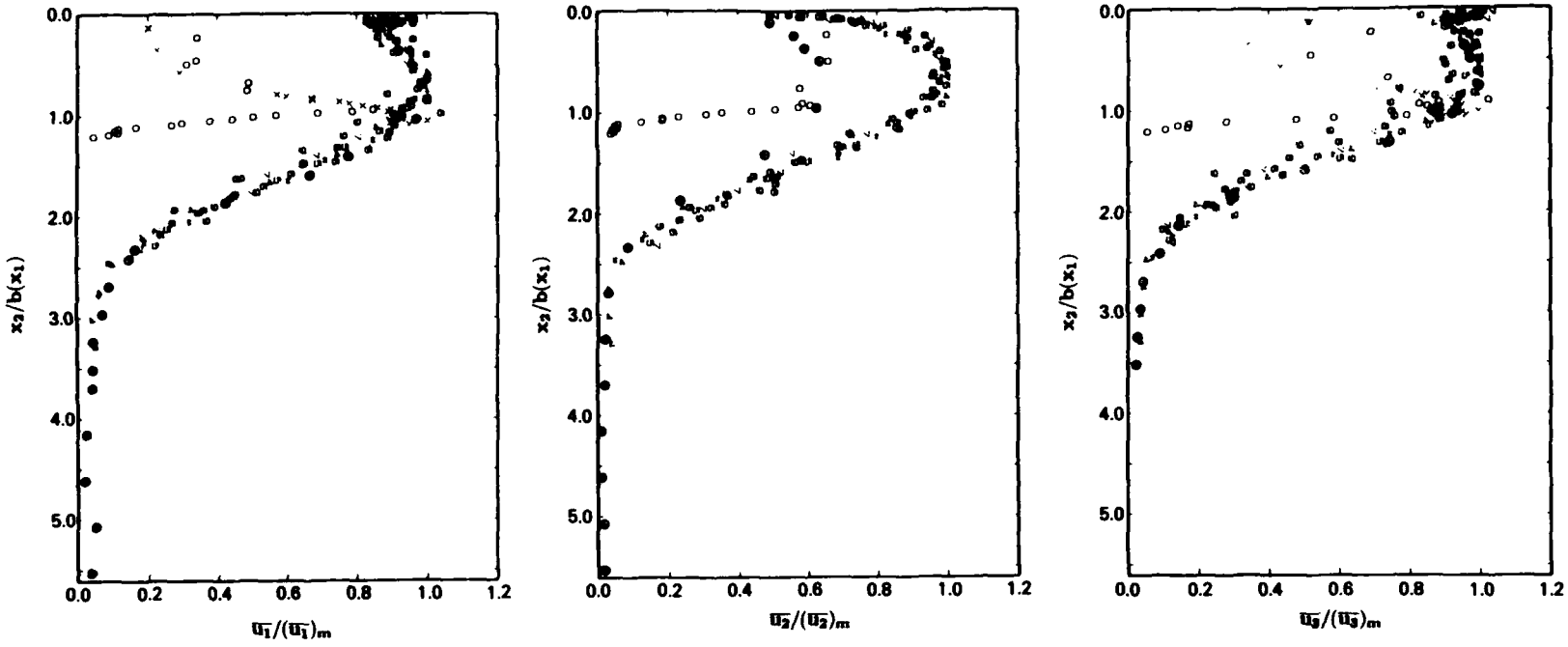

a) longitudinal b) vertical c) lateral

Fig. 13 – Turbulent intensity distributions at longitudinal measurement stations for the developing jet normalized by the local maximum.

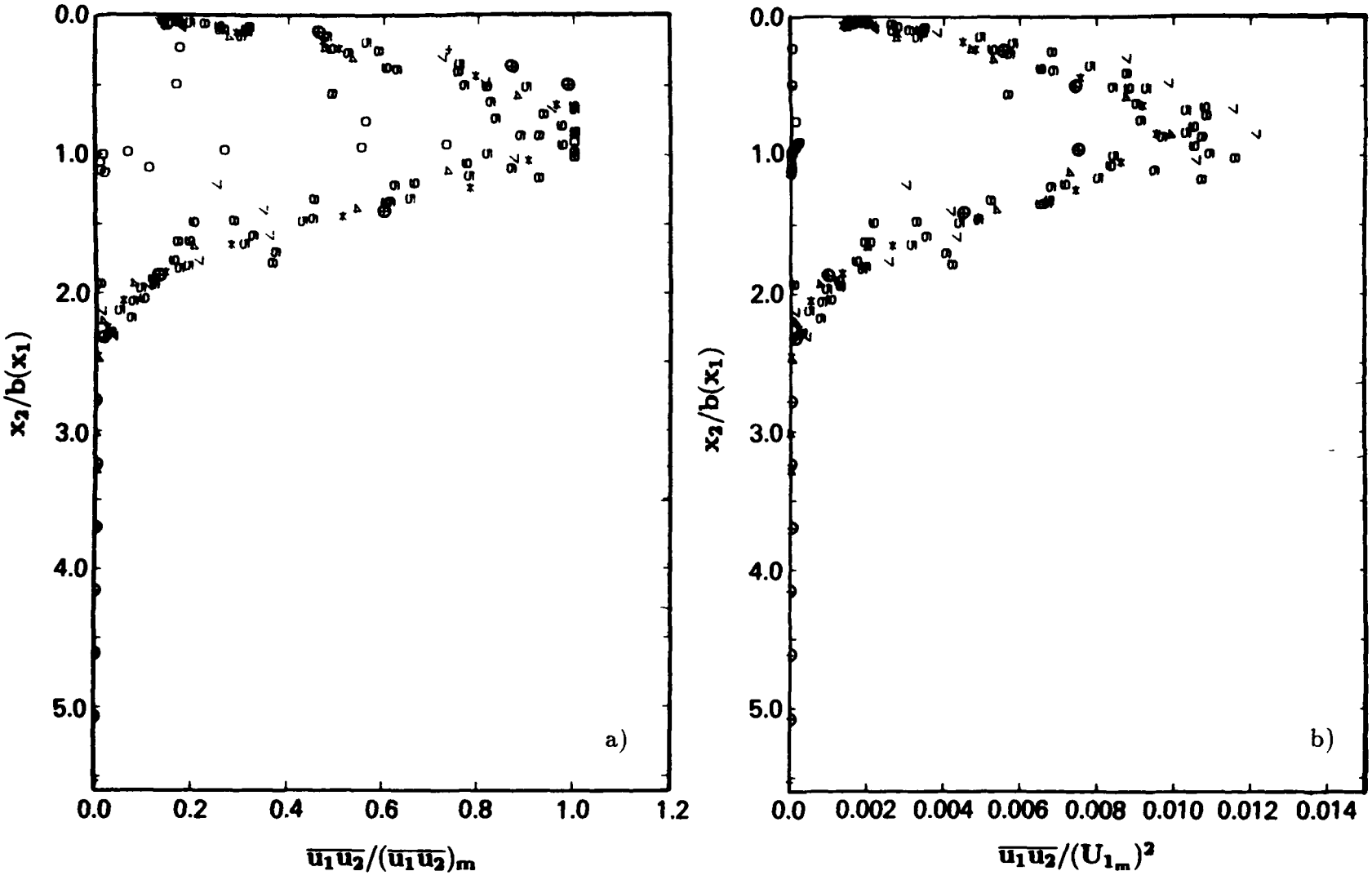

Fig. 14 – Turbulent shear stress distribution at longitudinal measurement stations for the developing jet normalized by a) the local maximum shear, b) the local velocity maximum.

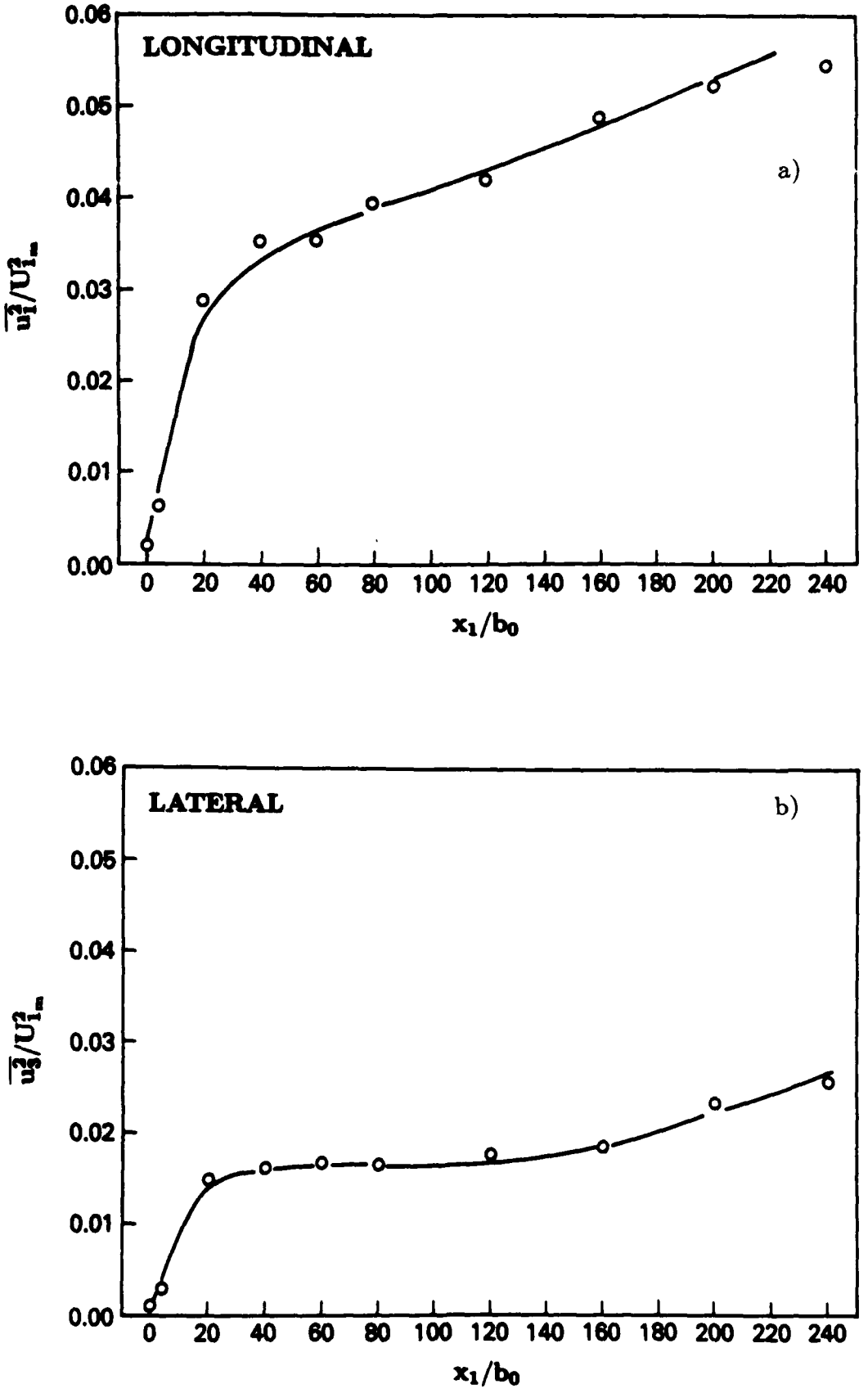

Fig. 15 – Longitudinal variations of maximum turbulent intensities.

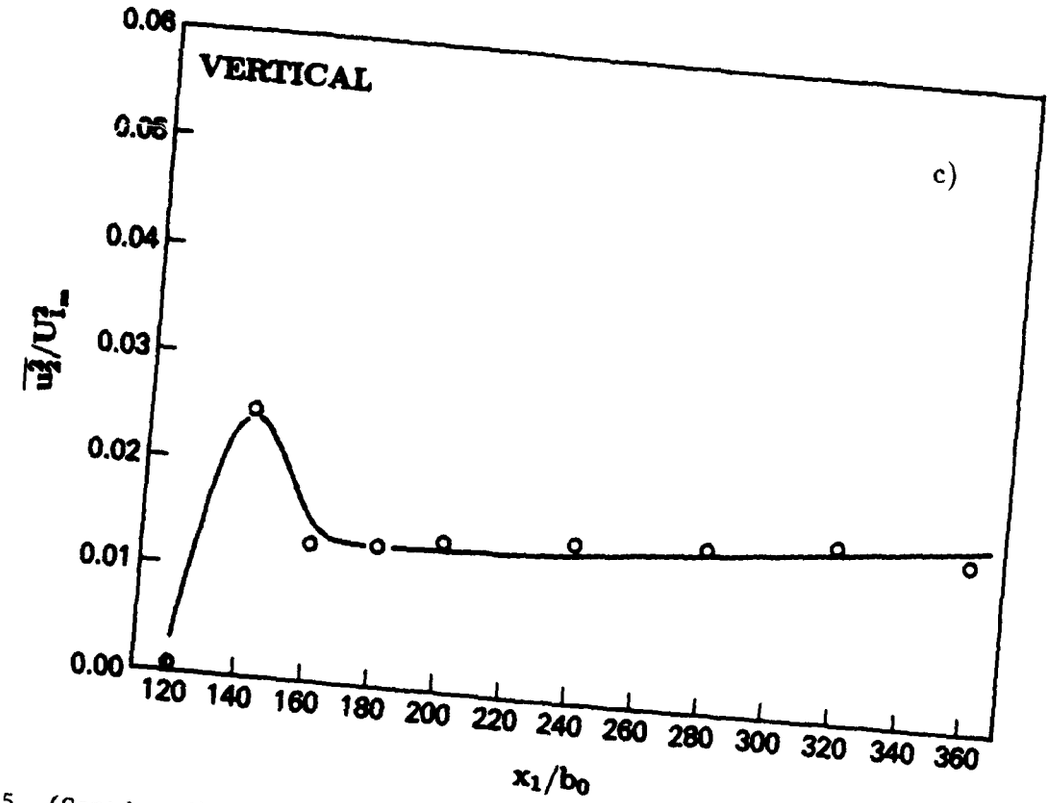

Fig. 15. (Continued) - Longitudinal variations of maximum turbulent intensities.

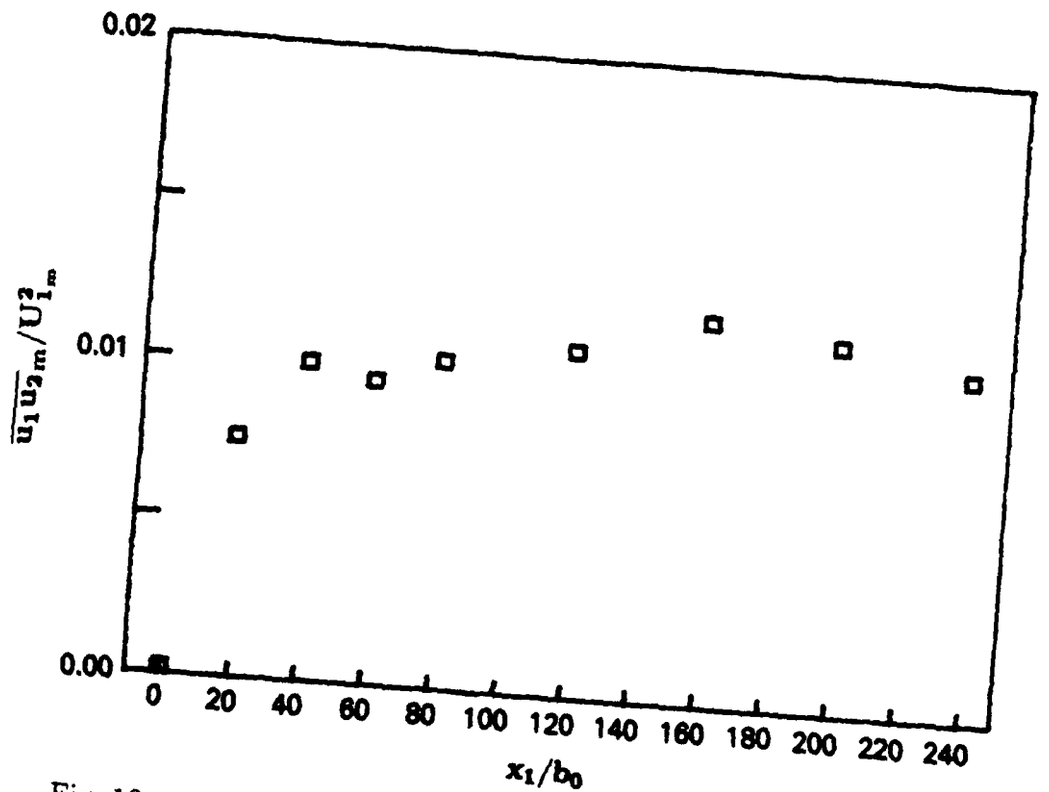

Fig. 16 – Longitudinal variation of maximum turbulent shear stress.

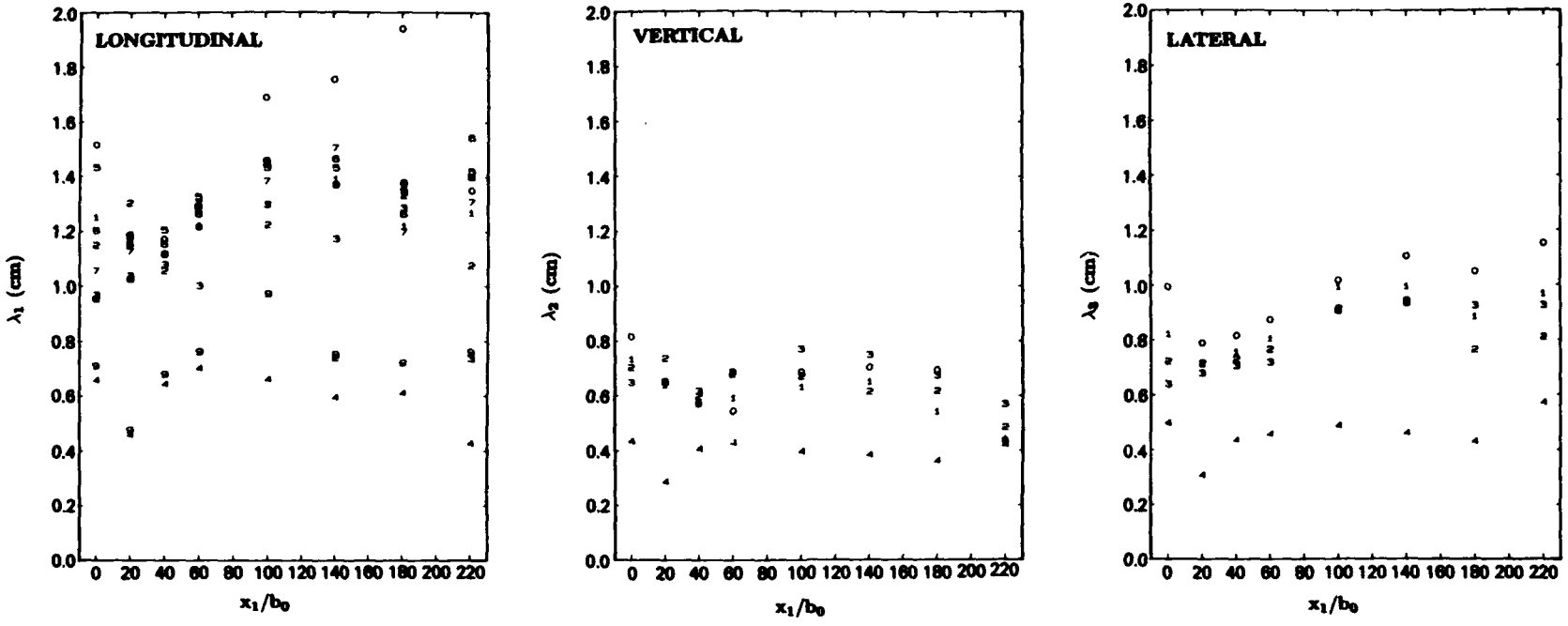

a) b) c)

Fig. 17 – Longitudinal variations of turbulent microscale estimates.

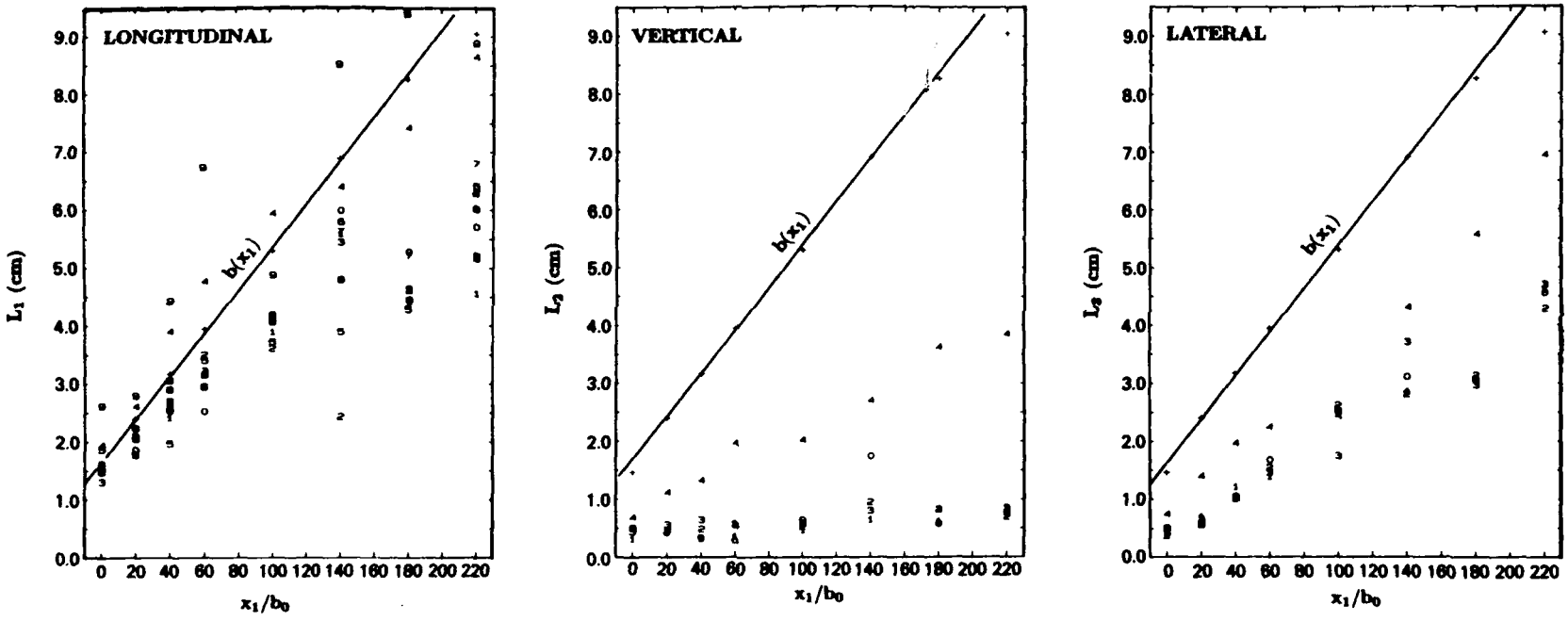

a) b) c)

Fig. 18 – Longitudinal variations of turbulent integral scale estimates.

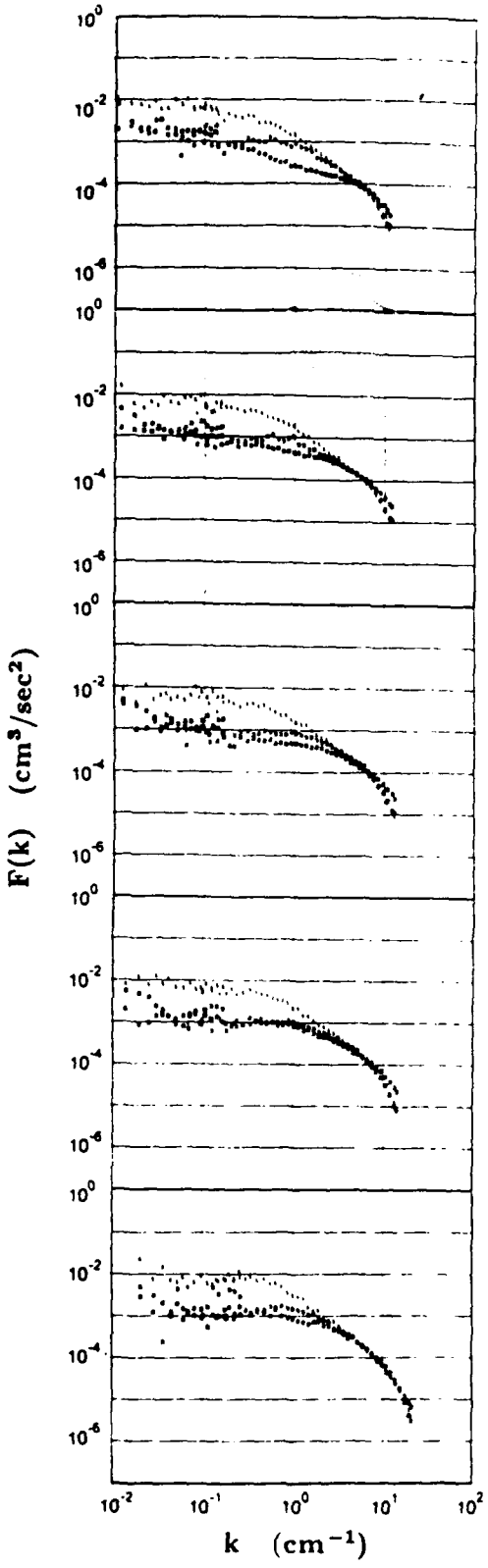

Fig. 19 – Turbulence spectra at $x_1/b_0 = 20$.

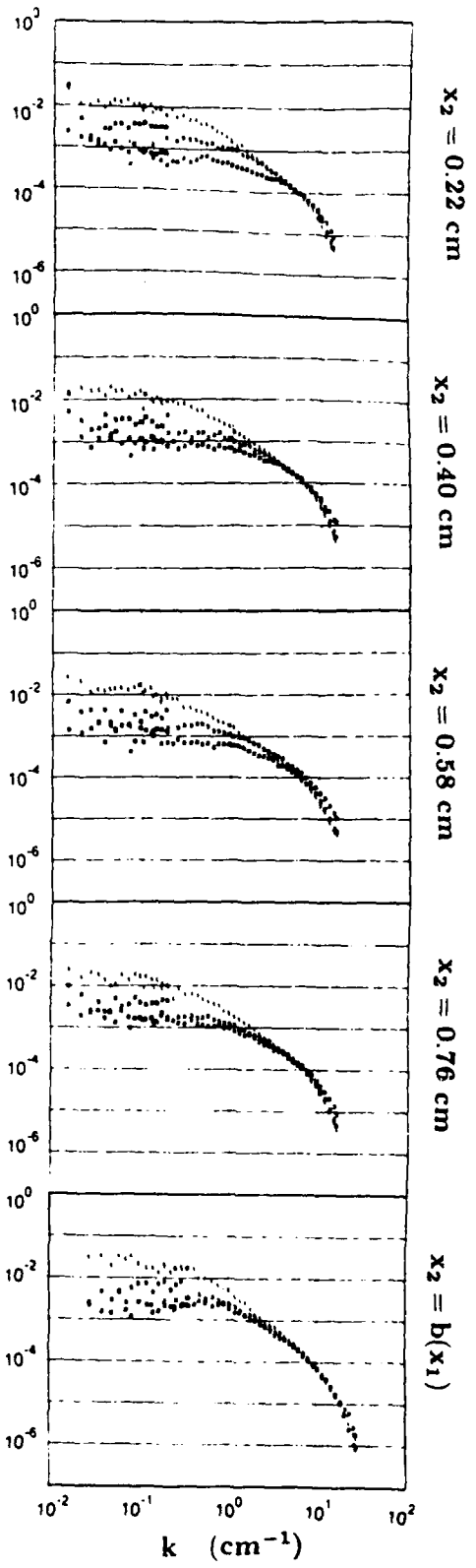

Fig. 20 – Turbulence spectra at $x_1/b_0 = 40$.

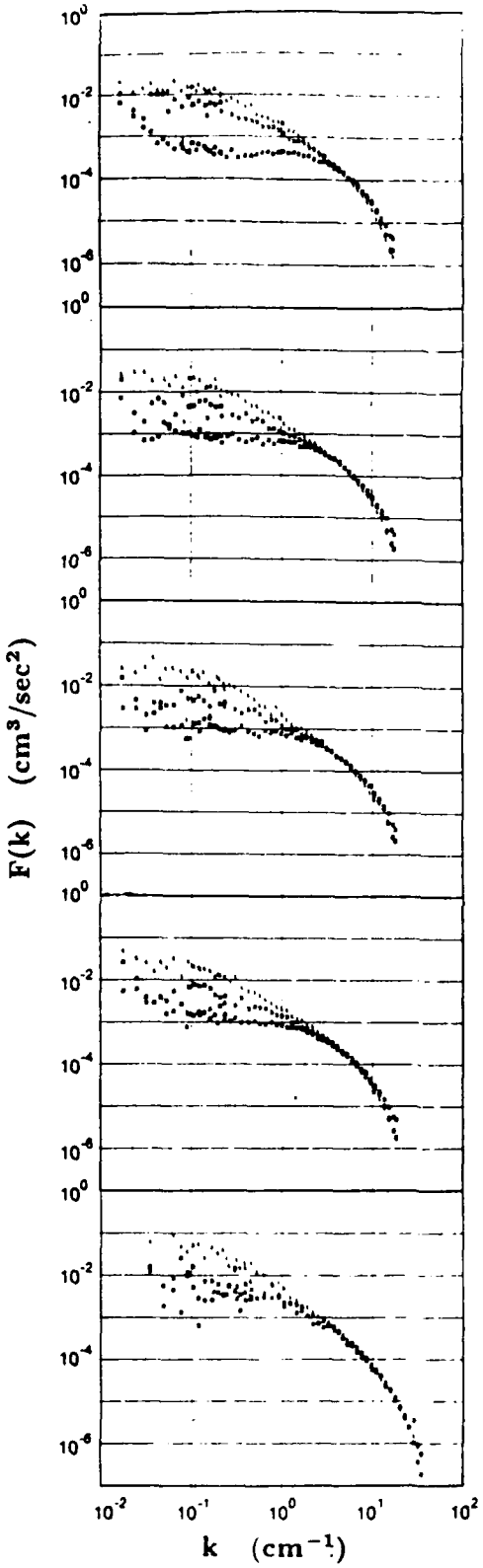

Fig. 21 – Turbulence spectra at $x_1/b_0 = 60$.

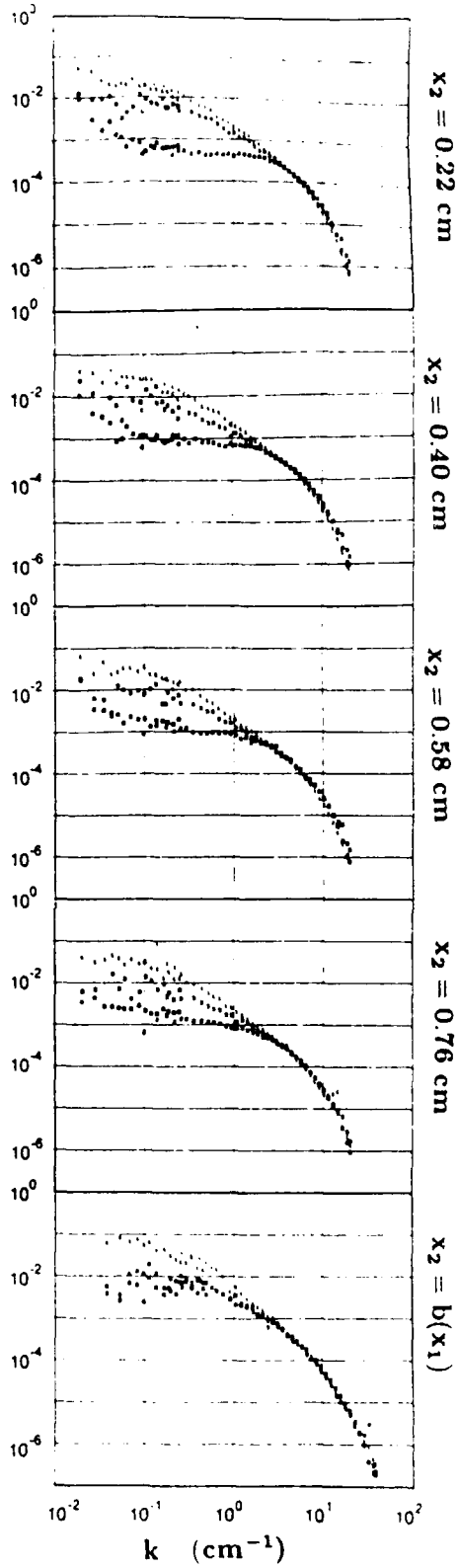

Fig. 22 – Turbulence spectra at $x_1/b_0 = 80$.

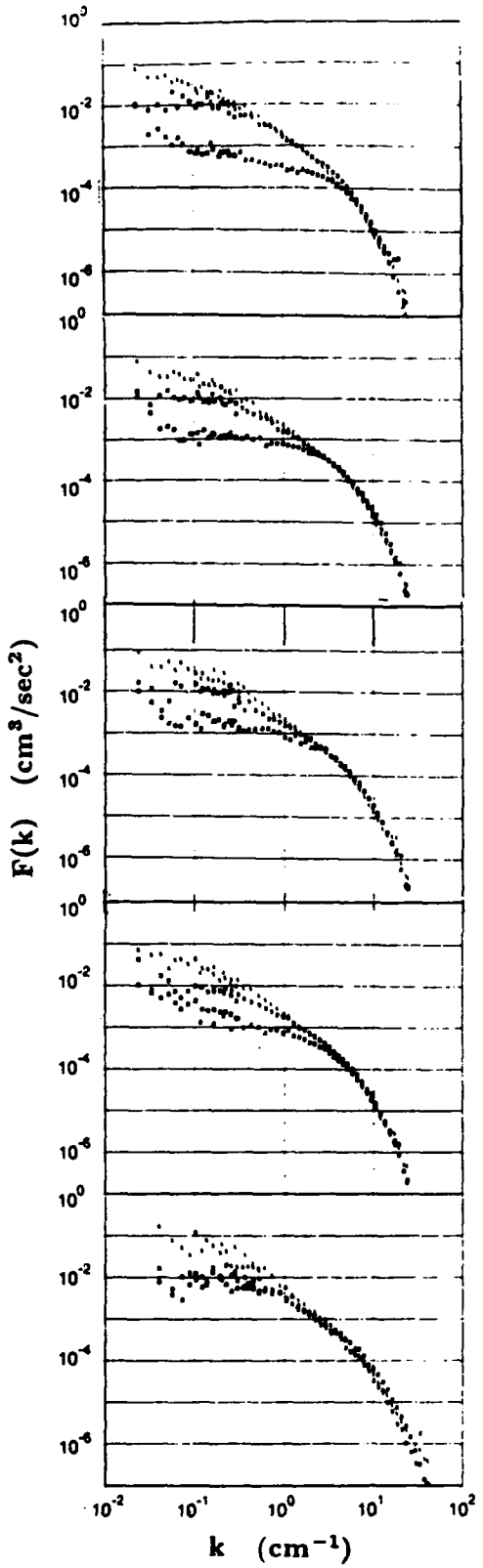

Fig. 23 – Turbulence spectra at $x_1/b_0 = 120$.

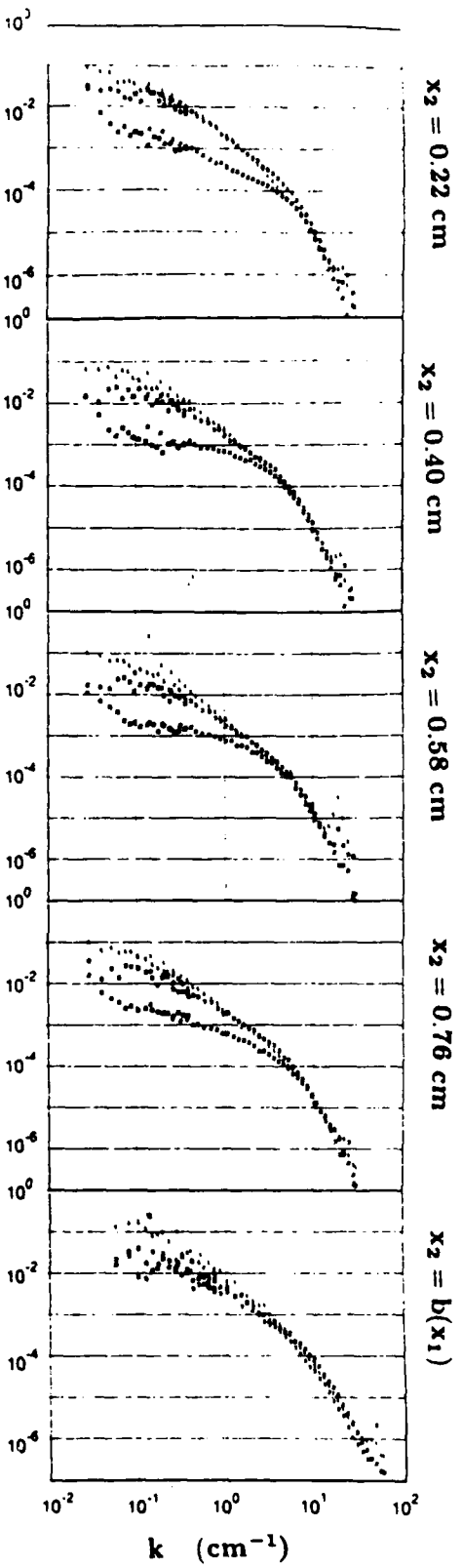

Fig. 24 – Turbulence spectra at $x_1/b_0 = 160$.

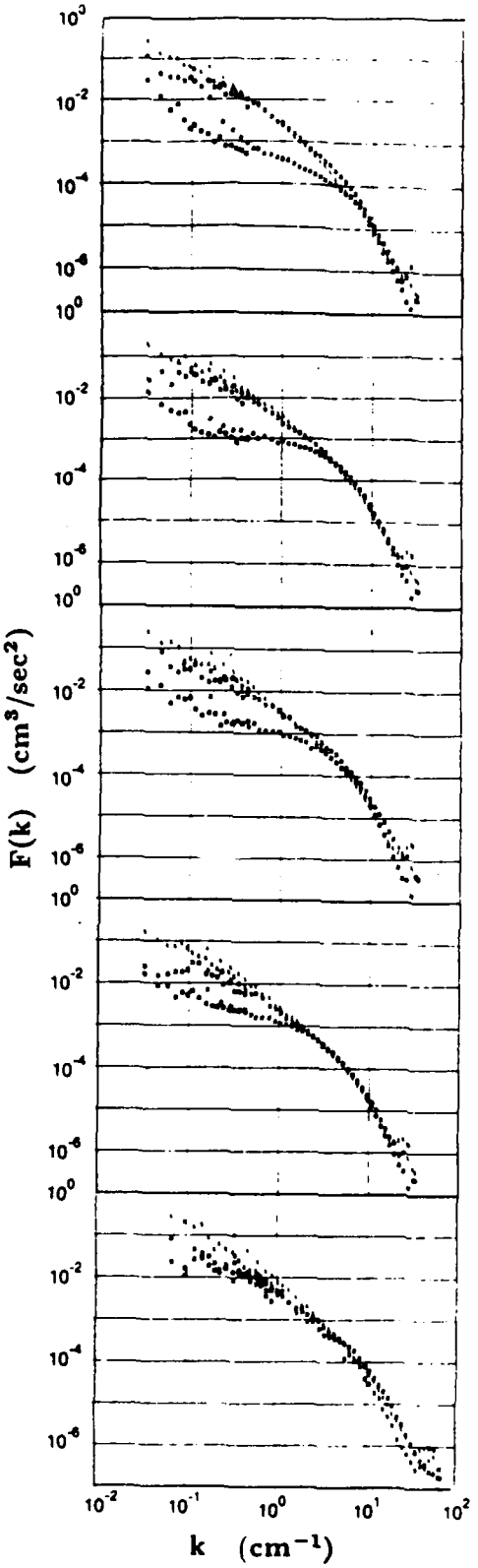

Fig. 25 – Turbulence spectra at $x_1/b_0 = 200$.

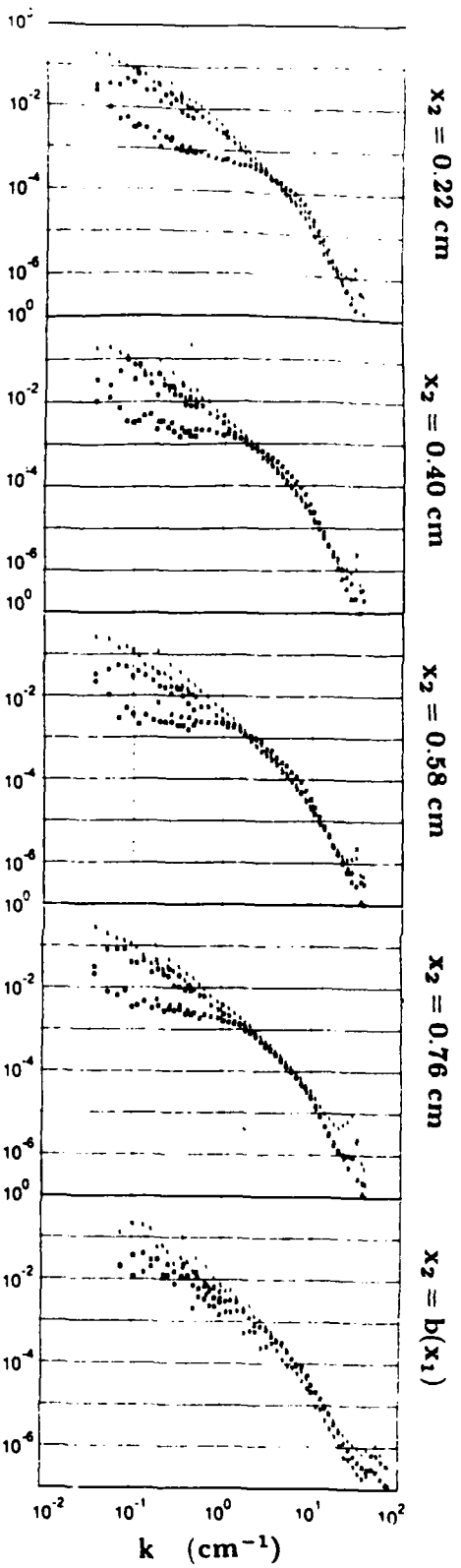

Fig. 26 – Turbulence spectra at $x_1/b_0 = 240$.

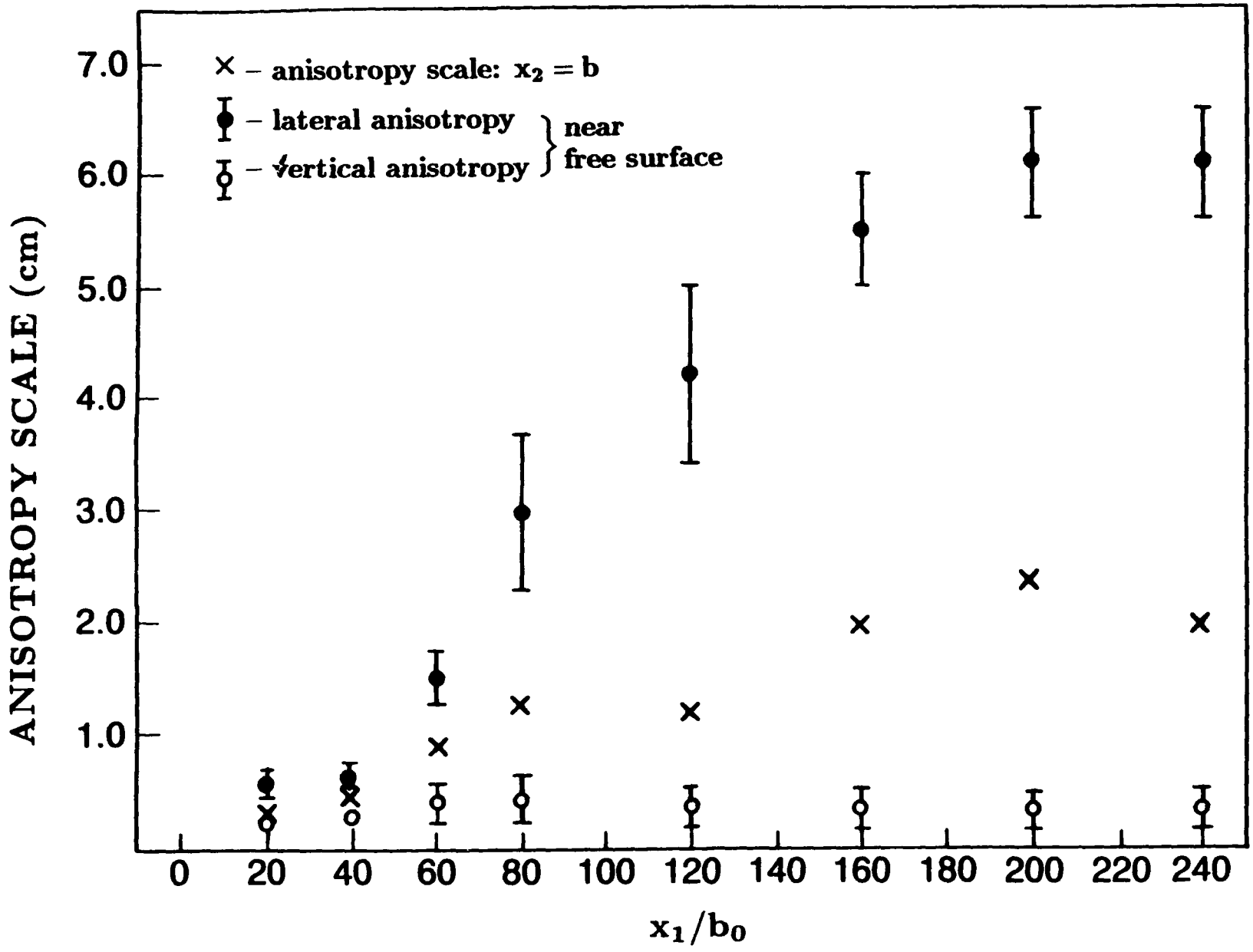

Fig. 27 – Smoothed estimates of cut-off scales for isotropy in turbulent spectra.